

University of Alberta

**Conformations of Some Amino Acids in Aqueous Solutions by Vibrational Circular
Dichroism Spectroscopy**

by

PeiYan Zhu

A thesis submitted to the Faculty of Graduate Studies and Research
in partial fulfillment of the requirements for the degree of

Master of Science

Department of Chemistry

©PeiYan Zhu

Fall 2012

Edmonton, Alberta

Permission is hereby granted to the University of Alberta Libraries to reproduce single copies of this thesis and to lend or sell such copies for private, scholarly or scientific research purposes only. Where the thesis is converted to, or otherwise made available in digital form, the University of Alberta will advise potential users of the thesis of these terms.

The author reserves all other publication and other rights in association with the copyright in the thesis and, except as herein before provided, neither the thesis nor any substantial portion thereof may be printed or otherwise reproduced in any material form whatsoever without the author's prior written permission.

Abstract

Vibrational circular dichroism (VCD) spectroscopy has been utilized to reveal the detailed conformational distributions of the dominant serine species and leucine species in aqueous solutions under three representative pH conditions, together with vibrational absorption (VA) spectroscopy, density functional theory (DFT), and molecular dynamics simulation. For both serine and leucine, the experimental VA and VCD spectra in H₂O and D₂O in the finger-print region at three pHs have been obtained. DFT calculations at the B3LYP/6-311++G(d,p) level have been carried out for the protonated, zwitterionic, and deprotonated species. In the leucine case, preliminary results based on the comparison of the experimental VA spectra of leucine in H₂O and D₂O in the finger-print region to the simulated spectra of different leucine species in the gas phase and with the polarizable continuum model (PCM) are presented. In the serine case, the comparison between the gas phase simulations and the experimental VA and VCD spectra suggests that one or two of the most stable conformers of each species contribute predominantly to the observed data, although some discrepancies have been noted. To account for the solvent effects, both the polarizable continuum model and the explicit solvation model have been considered. The hydrogen-bonded protonated, zwitterionic, and deprotonated serine-(water)₆ clusters have been constructed based on the radial distribution function analyses and molecular dynamics snap shots. Geometry optimization and VA and VCD simulations have been performed for these clusters at the B3LYP/6-311++G(d,p) level. The

detailed conformational distributions of the dominant serine and leucine species at three pHs have been investigated using VA and VCD spectroscopy together with ab initio calculations. Inclusion of the explicit water molecules has been found to improve the agreement between theory and experiment noticeably in all three cases, thus enabling conclusive conformational distribution analyses of serine in aqueous solutions directly.

Acknowledgements

First, I want to thank you for my supervisor Dr. Yunjie Xu. During my research study, her guidance and encouragement helps me to complete my study. Each time I lost myself in my research, she points out the direction to me. Some of my tough times, she encourages me and pulls me out of my passive emotion. Dr. Xu is very patient and warm-hearted. She always takes care of us, not only in our research area, but also in our daily life. Especially, during my pregnancy, I don't think I can make my study finished without her support and help. After a few years, I learned a lot from Dr. Xu. Her scientific way of thinking makes me study logically. Her kindness makes my life full of sunshine. Each of her constructive comments makes my study in my graduate school very challenging and enjoyable.

I want to also give my special thank you to the previous group member Dr. Guochun Yang. He introduces me to my first project in this research group. Without any doubt, he is the person who answers my most theoretical calculations questions. He is very friendly and helpful from the early stage of my research project. Further, I also want to express my warm thanks to every group members in Dr. Xu and Dr. Jäger's group. They are all very friendly and helpful in both my research and personal life, and that makes all of us good friends and research colleagues.

For this thesis work, I also want to thank Dr. John Klassen, and Dr. Jingli Luo. As my master defense examiners, their questions make me feel much clear on my projects. I am really

appreciating their time to mark the corrections to my thesis. I really want to thank you for their carefulness and supportive.

Finally, I want to give a great thank you to my husband, especially during my pregnancy. He always shows his understanding and supporting with his endless love throughout my life. He is a big fun in my research, and he always encourages me to study more in my research area. I will hardly complete my degree, if he is not with me in my life.

Table of contents

Chapter	Page
Chapter 1	
Introduction	1
References.....	4
Chapter 2 Theoretical and Experimental Methods	5
2.1 Ab initio Calculations.....	5
2.2 FTIR-VCD Module.....	6
References.....	12
Chapter 3 Conformations of Serine in Aqueous Solutions as Revealed by Vibrational Circular Dichroism	14
3.1 Introduction.....	14
3.2 Experimental and Theoretical Details.....	17
3.2.1 Experimental Methods.....	17
3.2.2 Computational Details.....	18
3.2.2.1 MD Simulation.....	18
3.2.2.2 DFT Calculations.....	19
3.3 Results and Discussions.....	20

3.3.1 Experimental VA and VCD spectra.....	20
3.3.2 Simulations of the VA and VCD Spectra of Monomeric Conformers of Neutral, Zwitterionic, Protonated and Deprotonated Serine.....	26
3.3.3 Explicit and Continuum Salvation Models of the Zwitterionic, Deprotonated, and Protonated Serine with Water.....	34
3.4 Conclusions.....	45
References.....	49
Chapter 4 Preliminary Results of the Conformational Analysis of Leucine in Water..	53
4.1 Introduction.....	54
4.2 Experimental Methods.....	54
4.3 Computational Details.....	54
4.4 Results and Discussions.....	54
4.4.1 Experimental VA and VCD spectra.....	54
4.4.2 Calculations of the VA and VCD Spectra of the Leucine-water Clusters.....	58
4.4.2.1 Conformers of Neutral, Protonated and Deprotonated Leucine in the Gas Phase.....	58
4.4.2.2 Conformers of Zwitterionic, Deprotonated, and Protonated Leucine With Water.....	64
4.5 Conclusion	73
References.....	74
Chapter 5 General Conclusions and future work	76

List of Tables

Table	Page
3.1 The relative total energies ΔE (kcal/mol) and the relative Gibbs free energies ΔG (kcal/mol) of the zwitterionic, deprotonated, and protonated serine-(water) ₆ clusters at the B3LYP/6-311++G(d,p) level of theory and their percentage Boltzmann distributions at room temperature.....	36
4.1 Summary of 27 neutral leucine structures calculated.....	59
4.2 The relative total energies ΔE (kcal/mol) and the relative Gibbs free energies ΔG (kcal/mol) of the zwitterionic, deprotonated, and protonated leucine with PCM of water at the B3LYP/6-311++G(d,p) level of theory and their percentage Boltzmann distributions.....	65
4.3 Summary of the possible zwitterionic leucine-water conformers.....	66

List of Figures

Figure	Page
2.1 Michelson interferometer.....	7
2.2 FTIR-VCD spectrometer.....	9
2.3 Circularly Polarized Light with Components Right Handed.....	10
2.4 Circularly Polarized Light with Components Left Handed.....	10
3.1 The experimental VA spectra of serine in water at a number of the different concentrations interval.....	21
3.2 The experimental VA and VCD spectra of <i>L</i> -serine in water at three different concentrations.....	22
3.3 Comparisons of the experimental VA and VCD spectra of <i>L</i> -serine in H ₂ O at three different pH values.....	24
3.4 Comparisons of the experimental VA and VCD spectra of <i>L</i> -serine in D ₂ O at three different pD value.....	25
3.5 Simulated VA and VCD spectra of the four most stable neutral serine conformers at the B3LYP/6-311++G(d,p) level.....	27
3.6 Optimized geometries of the four lowest energy conformers of the zwitterionic, deprotonated, and protonated monomeric serine conformers at the B3LYP/6-311++G(d,p) level.....	28
3.7 Simulated VA and VCD spectra of the four most stable zwitterionic serine and of the two most stable deuterated zwitterionic serine conformers at the B3LYP/6-311++G(d,p) level.	29
3.8 Simulated VA and VCD spectra of the four most stable deprotonated serine and of the two most stable deuterated deprotonated serine conformers at the B3LYP/6-311++G(d,p) level.....	30

3.9 Simulated VA and VCD spectra of the four most stable protonated serine and of the two most stable deuterated protonated serine conformers at the B3LYP/6-311++G(d,p) level.....	30
3.10 Optimized geometries of the five most stable zwitterionic, deprotonated, and protonated serine-(water) ₆ clusters at the B3LYP/6-311++G(d,p) level.....	38
3.11 Comparisons of the simulated VA and VCD spectra of the five most stable zwitterionic serine-(water) ₆ conformers and the zwitterionic serine in the PCM of water with the related experimental data in water at the neutral pH.....	40
3.12 Comparisons of the simulated VA and VCD spectra of the five most stable deprotonated serine-(water) ₆ conformers and the deprotonated serine in the PCM of water with the related experimental data in water at the pH=13.....	43
3.13 Comparisons of the simulated VA and VCD spectra of the five most stable protonated serine-(water) ₆ conformers and the protonated serine in the PCM of water with the related experimental data in water at the pH=1.....	44
S1 Optimized geometries of the twelve lowest energy conformers of the serine monomer at the B3LYP/6-311++G(d,p) level.....	51
S2 RDFs obtained from the MD simulation of the zwitterionic serine species in water.....	52
4.1 Comparisons of the experimental VA spectra of <i>L</i> -leucine in H ₂ O at three different pH values.....	56
4.2 Comparisons of the experimental VA spectra of <i>L</i> -leucine in D ₂ O at three different pD values.....	57
4.3 Optimized geometries of the three lowest energy conformers of the zwitterionic, deprotonated, and protonated monomeric leucine conformers at the B3LYP/6-311++G(d,p) level.....	63
4.4 Simulated VA spectra of PCM of the three most stable zwitterionic leucine and the three most stable deuterated zwitterionic leucine conformers at the B3LYP/6-311++G(d,p) level.	69
4.5 Simulated VA spectra of PCM of the three most stable protonated leucine and the three most stable deuterated protonated leucine conformers at the B3LYP/6-311++G(d,p) level.....	70
4.6 Simulated VA spectra of PCM of the three most stable deprotonated leucine and the three most stable deuterated deprotonated leucine conformers at the B3LYP/6-	

311++G(d,p) level.....	71
4.7 Comparison of VCD spectra of leucine in D ₂ O using PCM of leucine with water.....	72

Chapter 1 Introduction

Chirality was first defined by Lord Kelvin: “I call any geometrical figure, or group points, chiral, and say that it has chirality, if its image in a plane mirror, ideally realized, cannot be brought to coincide with itself.” A chiral molecule has a mirror image which is not superposable onto itself.¹ Our left and right hands are the most common chiral objects we encounter in our daily life. They are mirror images to each other. But we cannot put them on top of other to make them coincide exactly.

A chiral object can recognize the chirality of another chiral entity. In 1884, the famous “lock and key” principle was proposed by Fisher to explain the specific recognition between enzyme and substrate in biochemical reactions.² Since then, many researchers have studied such recognition processes at the molecular level in order to understand the intramolecular and intermolecular interactions involved quantitatively.³ Similarly, a chiral sample interacts differently with the right and left circularly polarized light or ‘chiral’ light. This leads to the phenomenon of circular dichroism. Vibrational circular dichroism (VCD) spectroscopy measures the differential absorption of a chiral sample of the right versus the left circularly polarized light, accompanying a vibrational transition. For all vibrational modes of a chiral molecule, there are the associated VCD spectral peaks with different intensity and sign. Therefore, VCD measurements provide chiral spectral signatures in the finger print region for all chiral molecules. In recent years, VCD spectroscopy has emerged as a powerful new method for the

determination of absolute configurations of chiral molecules in solution and for the study of their conformational distributions in solution.

In this thesis work, I have applied VCD spectroscopy in combination with ab initio theoretical modelling to investigate the conformational distributions of two amino acids, namely serine and leucine, in water solution. Serine and leucine are natural amino acids and are fundamental building blocks for proteins and other biomolecules. For example, serine participates in the catalytic function of many enzymes,⁴ while leucine is utilized in the liver, adipose and muscle tissues.⁵ Different conformations adopted by an amino acid unit may strongly influence the functionality of proteins and large biomolecules. Since most biologically relevant reactions involving natural amino acids happen in environments which have water present, it is important to probe such their conformational distributions directly in solution. In water, the strong hydrogen bonding interactions between chiral solute and water molecules are likely to influence the intramolecular hydrogen-bonding interactions in the chiral solute molecule. As a result the preferred conformation of a particular amino acid might alter significantly. Therefore, the solvent effects, in particular, the hydrogen-bonding interactions between solute and water are the main interest in my study.

In my study, I have measured vibrational absorption (VA) and VCD spectra of serine and leucine in water solution under three representative pH conditions, i.e. highly acidic, neutral, and basic conditions. At the same time, the density functional theory (DFT) has been used as the theoretical tool to search for the dominant conformations of both amino acids under three corresponding pH conditions in solution. The final conclusions have been achieved by

comparing the simulated VA and especially VCD spectra with the experimental data. Insights into the intramolecular and intermolecular interactions of serine and leucine in water solution have been gained.

In the next chapter, I will give a brief review of the theoretical background and the VCD instrumentation. In Chapter 3 and Chapter 4, I will discuss my two projects with serine and leucine, respectively. A general conclusion is presented at the end of my thesis.

References:

1. T.W. Graham Solomons, Craig B. Fryhle. (2004). Solomons & Fryhle Organic Chemistry Eighth Edition. John Wiley & Sons, Inc.
2. Fisher, E. *Ber. Dtsch. Chem. Ges.* 1984.27. 2985.
3. Schneider, H. J. *Methods and Principles in Medicinal Chemistry*, 2003, 19, 21
4. Karlheinz Drauz, Ian Grayson, Axel Kleemann, Hans-Peter Krimmer, Wolfgang Leuchtenberger, Christoph Weckbecker (2005), "Amino Acids", *Ullmann's Encyclopedia of Industrial Chemistry*, Weinheim: Wiley-VCH, doi:10.1002/14356007.a02_057.pub2
5. J. Rosenthal, A. Angel, J. Farkas, Department of Medicine, University of Toronto, Toronto, Canada. "Metabolic fate of leucine: A significant sterol precursor in adipose tissue and muscle". *American Journal of Physiology* Vol. 226, No. 2, p. 411-418.
<http://ajplegacy.physiology.org/cgi/reprint/226/2/411>. Retrieved 2008-03-25.

Chapter 2

Theoretical and experimental methods

2.1 *Ab initio* calculations

High level *ab initio* calculations have been used in my study in order to search possible conformational conformers and to simulate the corresponding IR and VCD spectra of the interested systems. All these calculations have been carried out using Gaussian 03 program package.¹ In my thesis projects, all geometry optimizations of possible conformations and harmonic frequency calculations, as well as the IR and VCD intensity calculations have been carried out using Density Functional Theory (DFT).² The DFT method has been widely accepted as a cost-effective approach to optimize molecular structures in vibrational, NMR, and UV studies. The B3LYP³ hybrid functional was chosen for all calculations reported in this thesis because of its proven reliability in describing strong hydrogen bonded complexes⁴ and in predicting VA frequencies and VA and VCD intensities.⁴ It was reported before that the interaction energies of the C-H...O and O-H...O interactions depended on the basis sets used.⁶ This issue has been addressed in detail in a number of references.⁷ The 6-311++G(d,p) basis set was adopted in my study because it has been used successfully to describe many properties of hydrogen bonded systems.⁸

In all geometry optimizations, the tight convergence criteria were used to ensure the significance of small bond length differences. The true minimum nature of the optimized

geometries was confirmed by the frequency calculation that all vibrational frequencies obtained are real. The intensity of a vibrational transition from the ground vibrational level to the first excited vibrational level in the ground electronic state is calculated as:

$$D(g - e) = |\langle g | \vec{\mu}_{el} | e \rangle|^2 \quad (2.1)$$

where g represents the ground vibrational level, e denotes the first excited level, and $\vec{\mu}_{el}$ is the electronic dipole moment operator. The intensity of a VCD peak is calculated using the following formula.

$$R(g - e) = \text{Im}[\langle g | \vec{\mu}_{el} | e \rangle] \bullet [\langle e | \vec{\mu}_{mag} | g \rangle] \quad (2.2)$$

where g , e , and $\vec{\mu}_{el}$ are similarly defined as in equation (2.1) while $\vec{\mu}_{mag}$ is the magnetic dipole moment operator and Im indicates imaginary.

2.2 FTIR-VCD Module

A Fourier Transform Infrared (FTIR) spectrometer, Vertex 70, equipped with a VCD module, PMA 50, was used to record the VA and VCD spectra in this thesis. Both modules are from Bruker Instrument. The main part of the FTIR module is a Michelson Interferometer. As shown in Figure 2.1, the infrared light source passes through a beam splitter, and is split into two beams: 50% to the fixed mirror and 50% to the moving mirror.⁹ After that, the light beams reflected from the two mirrors are recombined at the beam splitter and then go through the sample and finally go to the detector. Depending on the path difference of the two optical arms,

constructed and destructed interference is generated and an interferogram is recorded as a function of the distance travelled by the mirror. FT of the data collected then provides the vibrational absorption spectrum as a function of wavenumber. When no sample is placed in the beam, the interferogram is affected by the variation of source intensity and splitter efficiency with wavelength. In order to get the spectra with minimum window's interference in the desirable wavenumber region, a pair of BaF₂ (Barium Fluoride) windows is used to hold the sample solution with a Teflon spacer in between the two windows.

The VCD optical bench, PMA 50,^{10, 11} which is attached to the FTIR module, is used to record the VCD spectra. The same light beam from the FTIR spectrometer after the interferometer is redirected to go to the VCD module instead of through the sample in the FTIR sample chamber. As shown in Figure 2.2, the light source from FTIR passes through an optical filter with a cut off at 1800 cm⁻¹, a linear polarizer, a photoelastic modulator (PEM), the chiral sample, and finally to an IR detector which is cooled by liquid nitrogen to reduce the noise level.

The PEM is controlled by a driver and is modulated with a 50 kHz frequency. This PEM is used to generate right and left circularly polarized light with a modulation frequency of 50 kHz. The linear polarizer and the PEM are aligned, so that the polarized light reaches the PEM at 45 degree to the modulator axis. The unpolarized light passes through the linear polarizer and becomes linearly polarized. This linearly polarized light can be decomposed into two orthogonal components: one with its electric vector parallel to the PEM axis and the other one perpendicular to it. Due to the stretches and compresses of the modulator, the speeds of light in these two different directions are retarded differently. More specifically, when the PEM

compresses, the perpendicular light component is retarded, while the parallel one does not. On the other hand, when the PEM stretches, the parallel light component is retarded, while the perpendicular one does not. Therefore, the parallel light component is ahead of the perpendicular one when the PEM compresses and the perpendicular light component is ahead of the parallel one when the PEM stretches. The light becomes right circularly polarized if the two phase difference is exactly 90 degree between the perpendicular and parallel components and the light becomes left circularly polarized if the two phase difference is exactly 270 degree. The two situations described above are depicted described in Figure 2.3¹² and 2.4.¹³

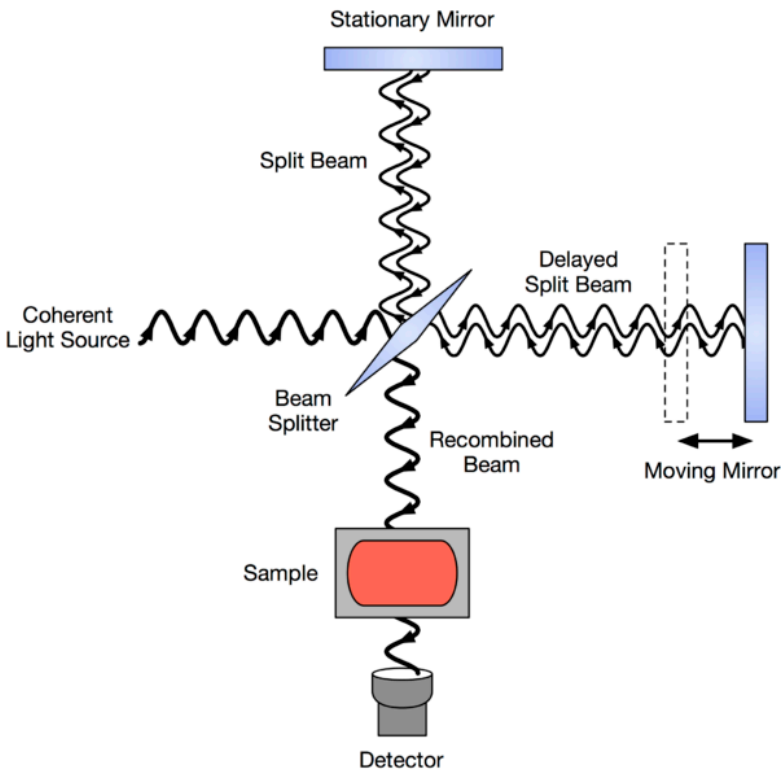


Figure 2.1 A schematic diagram of a Michelson interferometer (Taken from Ref. 9)

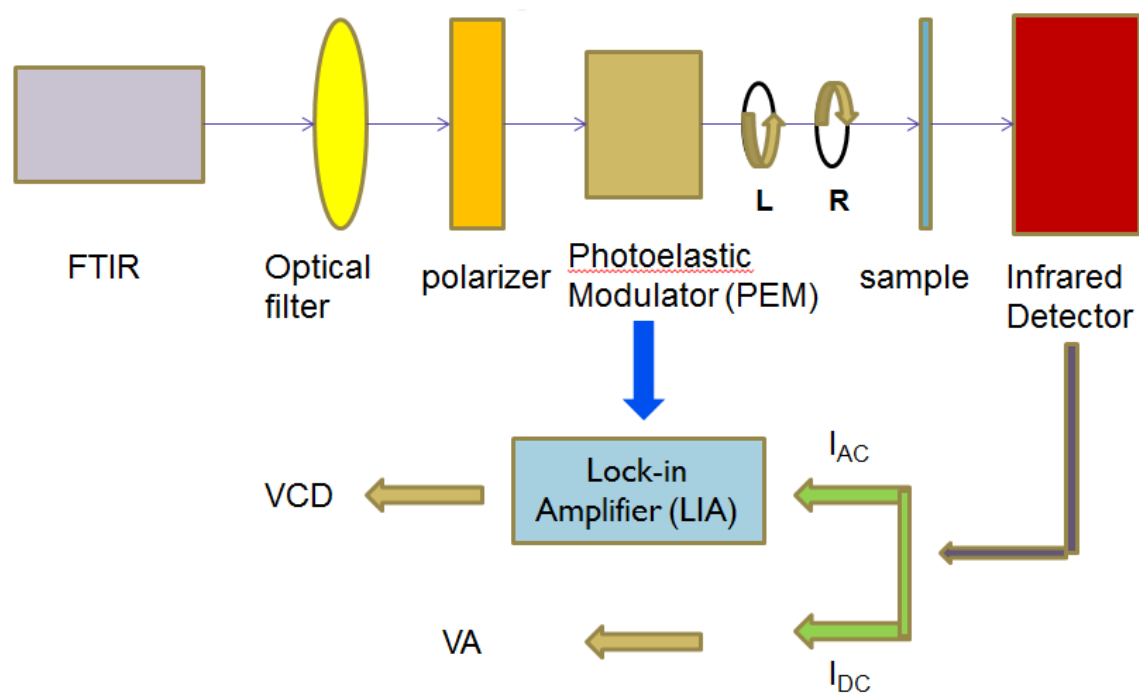


Figure 2.2 A schematic diagram of an FTIR-VCD spectrometer

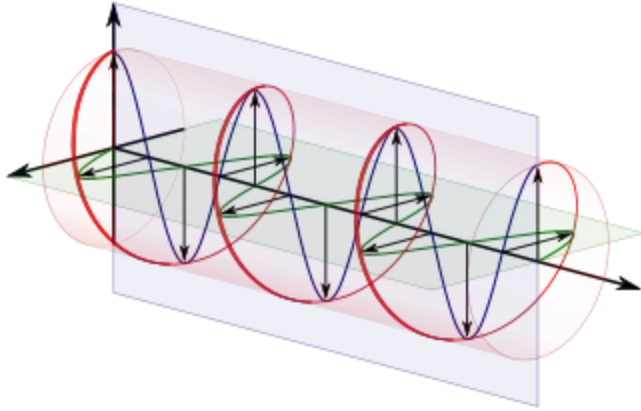


Figure 2.3 Right circularly polarized light with its two perpendicular components depicted.

(Taken from Ref. 12).

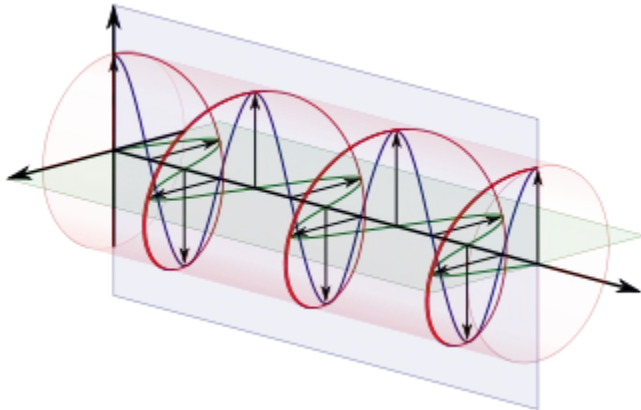


Figure 2.4 Left circularly polarized light with its two perpendicular components depicted. (Taken

from Ref. 13).

After the PEM, the light passes through the sample cell which contains either *L* or *D* enantiomers. Due to the nature of a chiral molecule, it absorbs the left and right circularly light differently. The light collected at the detector is doubly modulated by the FTIR spectrometer and the PEM. The signal is processed in two ways. One part goes through a low-pass filter so that the modulation at the high frequency of 50 kHz is removed and this after FT produces the IR spectrum. The other part is sent to a lock-in amplifier and the signal is demodulated at the reference frequency of 50 kHz, and then FT to give us the VCD spectrum. Although the VCD signal is in general much weaker, about 10^4 to 10^6 times weaker, than the corresponding IR signal, it is possible to obtain a VCD spectrum with good signal-to-noise ratio with care and practice.

References:

1. Frisch, M. J.; Trucks, G. W.; Schlegel, H. B.; Scuseria, G. E.; Robb, M. A.; Cheeseman, J. R.; Montgomery, J. A., Jr.; Vreven, T.; Kudin, K. N.; Burant, J. C.; Millam, J. M.; Iyengar, S. S.; Tomasi, J.; Barone, V.; Mennucci, B.; Cossi, M.; Scalmani, G.; Rega, N.; Petersson, G. A.; Nakatsuji, H.; Hada, M.; Ehara, M.; Toyota, K.; Fukuda, R.; Hasegawa, J.; Ishida, M.; Nakajima, T.; Honda, Y.; Kitao, O.; Nakai, H.; Klene, M.; Li, X.; Knox, J. E.; Hratchian, H. P.; Cross, J. B.; Bakken, V.; Adamo, C.; Jaramillo, J.; Gomperts, R.; Stratmann, R. E.; Yazyev, O.; Austin, A. J.; Cammi, R.; Pomelli, C.; Ochterski, J. W.; Ayala, P. Y.; Morokuma, K.; Voth, G. A.; Salvador, P.; Dannenberg, J. J.; Zakrzewski, V. G.; Dapprich, S.; Daniels, A. D.; Strain, M. C.; Farkas, O.; Malick, D. K.; Rabuck, A. D.; Raghavachari, K.; Foresman, J. B.; Ortiz, J. V.; Cui, Q.; Baboul, A. G.; Clifford, S.; Cioslowski, J.; Stefanov, B. B.; Liu, G.; Liashenko, A.; Piskorz, P.; Komaromi, I.; Martin, R. L.; Fox, D. J.; Keith, T.; Al-Laham, M. A.; Peng, C. Y.; Nanayakkara, A.; Challacombe, M.; Gill, P. M. W.; Johnson, B.; Chen, W.; Wong, M. W.; Gonzalez, C.; Pople, J. A. Gaussian03, revision C.02; Gaussian, Inc.: Wallingford, CT, 2004.
2. Labanowski, J. K, Andzelm, J. W. *Density functional Methods in Chemistry*, Springer-Verlag: New York, 1991.
3. (a) A. D. Becke, *J. Chem. Phys.* 98, 5648 (1993). (b) C. T. Lee, W. T. Yang, R. G. Parr, *Phys. Rev. B-Condens. Matter.* 37, 785 (1988).
4. (a) P. J. Stephens, F. J. Devlin, C. F. Chabalowski, M. J. Frisch, *J. Phys. Chem.* 98, 11623 (1994). (b) T. Kuppens, W. Langenaeker, J. P. Tollenaere, P. Bultinck, *J. Phys. Chem. A* 107, 542 (2003). (c) T. Kuppens, K. van der Vandyck, J. Eycken, W. Herrebout, B. J. van der Veken, P. Bultinck, *J. Org. Chem.* 70, 9103 (2005). (d) T. Kuppens, W. Herrebout, B. van der Veken, P. Bultinck, *J. Phys. Chem. A* 110, 10191 (2006). (e) Ducasse, F. Castet, A. Fritsch, I. Huc, T. Buffeteau, *J. Phys. Chem. A* 111, 5092 (2007). T. Brotin, D. Cavagnat, J.-P. Dutasta, T. Buffeteau, *J. Am. Chem. Soc.* 128, 5533 (2006).
5. (a) W. Sander, M. Gantenberg, *Spectrochim. Acta A* 62, 902 (2005). (b) A. K. Chandra, S. Parveen. T. Zeegers-Huyskens, *J. Phys. Chem. A* 111, 8884 (2007). (c) J. N. Woodford, *J. Phys. Chem. A* 111, 8519 (2007). (d) P. I. Dem'yanov, R. M. Gschwind, *ORGANOMETALLICS*, 25, 5709 (2006).
6. Desiraju, G. R. *Chem. Commun. (Cambridge)* 2005, 24, 2995.
7. (a) Scheiner, S. *Hydrogen Bonding: A Theoretical Perspective*; Oxford University Press: New York, 1997. (b) Karpfen, A. Case studies in cooperativity in hydrogen-bonded clusters and polymers. In *Molecular Interactions. From Van der Waals to Strongly Bound Complexes*; Scheiner, S., Ed.; John Wiley & Sons: Chichester, UK, 1997; pp 265-296.

8. (a) Qian, W. L.; Krimm, S. J. Phys. Chem. A 2002, 106, 6628. (b) Kovacs, A.; Szabo, A.; Nemcsok, D.; Hargittai, I. J. Phys. Chem. A 2002, 106, 5671. (c) Kovacs, A.; Szabo, A.; Nemcsok, D.; Hargittai, I. J. Phys. Chem. A 2002, 106, 5671.
9. http://en.wikipedia.org/wiki/File:FTIR_Interferometer.png
10. FT-IR/VCD Manuals from Bruker Optics
11. Wang, B. Application note from Hinds Instruments.
12. http://en.wikipedia.org/wiki/File:Circular.Polarization.Circularly.Polarized.Light_With.Components_Right.Handed.svg
13. http://en.wikipedia.org/wiki/File:Circular.Polarization.Circularly.Polarized.Light_With.Components_Left.Handed.svg

Chapter 3

Conformations of Serine in Aqueous Solutions as Revealed by Vibrational Circular Dichroism

This chapter is directly copied from the published paper¹. I have done all experiments and some ab initio calculations and written the first draft of the paper. The molecular dynamics calculations were performed by Dr. Guochun Yang. M.R. Poopari did some of the calculations and Z. Bie, an undergraduate, was involved in this project at the early stage and did some preliminary measurements.

3.1 Introduction

Amino acids are bifunctional compounds which contain an amine and a carboxylic acid groups and have a side chain that varies among different amino acids.^{2,3} They are essential in life since they serve as building blocks of proteins and also often as intermediates in metabolism. Amino acids have attracted considerable attention from computational chemists because they contain a variety of intramolecular interactions and exhibit conformational topologies which are commonly found in biological systems and because they are amenable to

high-level *ab initio* calculations.⁴⁻⁷

Serine is one of the twenty naturally occurring amino acids and contributes significantly to the structures of proteins since it readily forms several hydrogen-bonds with other protein side groups.^{8,9} Recently, much attention has been paid to serine from both experimental and theoretical sides. Gronert and O'Hair had reported probably the most complete theoretical investigation of the potential energy surface of a neutral serine monomer. The authors surveyed a starting set of 324 conformers based on all possible combinations of the so called single-bond rotamers.⁴ In a subsequent Fourier transform (FT) infrared (IR) Ar-matrix study of the neutral serine monomer, Maes and coworkers¹⁰ interpreted their experimental data by using the simulated IR spectra of several lowest energy neutral conformers identified in Ref. 4. More recently, a number of theoretical studies¹¹⁻¹³ of the zwitterionic, protonated and anionic forms of serine were reported where their relative conformational stability and gas phase basicities and acidities were predicted. An FTIR study of serine in water under one pH condition confirmed that the dominant species is of zwitterionic form, although no detailed conformational study was performed.¹¹ Terahertz vibrational spectra of solid serine and cysteine amino acids were experimentally obtained and theoretically studied.¹⁴ Nafie and coworkers showed that it was possible to measure the vibrational circular dichroism (VCD) spectra of serine in D₂O¹⁵ and in the solid phase¹⁶ and found that the solid state VCD signals were considerably larger than those in solution. Serine has also been extensively investigated by using mass spectrometry in search of the origin of homochirality of life because the protonated serine octamers demonstrate a strong preference of homochirality.¹⁷ So far, most of the reported studies focused on serine in the gas phase or solid state. From a biological point

of view, it would be of substantial interest to gain detailed insights into the conformational properties of serine in water and its intermolecular hydrogen-bonding interactions with water since water is ubiquitous in life.¹⁸⁻²⁰

VCD spectroscopy measures the differential absorption of a chiral molecule to the left- and right-handed circularly polarized radiations in the IR region.²¹ VCD spectroscopy is highly sensitive to conformational changes of a chiral molecule and to its explicit hydrogen-bonding interactions with solvent molecules, for example, water. VCD spectroscopy can often provide more decisive discrimination among conformers than the conventional vibrational absorption (VA) spectroscopy which is also structurally sensitive.²² For example, it was utilized for conformational characterization of large biological samples, such as proteins and nucleic acids.²³⁻²⁶ In a series of recent studies, it was demonstrated that VCD spectroscopy combined with density functional theory (DFT) calculations could be used to uncover the explicit water solvent structures surrounding a chiral solute in aqueous solutions.²⁷⁻³⁰

In the present study, we have utilized VCD and VA spectroscopy together with DFT to investigate predominant species and conformations of serine at three representative pHs in both water and deuterated water. Extensive DFT calculations have been carried out for the low energy conformers of the neutral, zwitterionic, protonated, and deprotonated serine forms in the gas phase and in aqueous solutions using the polarizable continuum model (PCM).^{31,32} The explicit serine-water intermolecular hydrogen-bonding interactions have also been examined by using small explicit hydrogen-bonded serine-(water)₆ clusters built based on the snap shots from the molecular dynamics (MD) simulations and the analysis of the radius distribution functions (RDFs). The comparisons between the simulated and experimental VA and in

particular VCD spectra recorded in both H₂O and D₂O provide the decisive discrimination for reaching the conclusions for the conformational analyses.

3.2 Experimental and theoretical details

3.2.1 Experimental Methods

An FTIR spectrometer, Vertex 70, connected with a VCD optical bench, PMA 50, was used to record the VA and VCD spectra. The details of the instrument was described before.³⁰ For the current measurements, a pair of BaF₂ windows (International Crystal Laboratories) with variable path lengths was used. For the VCD measurements, a collection time of 180 to 240 minutes and a 4 cm⁻¹ resolution were applied. *L*- (99%) and *D*-serine (98%) were purchased from Sigma Aldrich and used without further purification. The doubly distilled water and D₂O (99.99%) from Sigma Aldrich were used as solvents. For the concentration dependence study, a series of VA spectra of *L*-serine in water were measured at concentrations ranging from 0.1 M to saturation and with a path length of 15 μm. To obtain reliable VCD measurements, it is highly desirable to maintain the VA absorption coefficients in the range of 0.2 to 0.8. To achieve this, the VCD spectra of *L*-serine at three representative concentrations of 1.0 M, 2.0 M, and 3.0 M were measured with a path length of 50, 25, and 15 μm, respectively. The VCD measurements of *L*-serine were corrected with the corresponding measurements of *D*-serine under identical experimental conditions to minimize any VCD artefacts.³³ No experiments were carried out with a racemic solution, given the fact that the racemic-serine has a much lower solubility in water. Serine can exist in water as several different species, such as the protonated, deprotonated, and zwitterionic species by tuning the solution pH values. Three representative pH values were

selected for the reasons further elaborated in Section 3.3.1. The pH values of 1.0 and 13.0 were achieved by adding a highly concentrated 6 M HCl solution and NaOH solution, respectively, whereas a pH of 5.68 was obtained experimentally when no strong acid or base was added. For simplicity and conciseness, we will refer to this condition where no strong acid or base was added as 'neutral' in the text from now on. Because the C=O stretching region is obscured by the strong absorption of water, further measurements in D₂O under the three pHs mentioned above have also been carried out. This allowed us to access the C=O stretching region in order to aid the VA band assignments and to identify the serine species and the most important conformers in water. In this case, 0.5 M *L*-serine in D₂O with a path length of 25 μm was used. For the pH = 1.0 and 13.0 solutions, a 6 M DCl and a 6 M NaOD solution were used to adjust the solution to the desired pDs, respectively, while a pD value of 5.68 was measured experimentally when no strong acid or base was added. The same VA and VCD correction procedures used for the H₂O solutions have also been applied for the D₂O measurements.

3.2.2 Computational Details

3.2.2.1 MD simulation

To survey the geometries of a large number of possible small serine-(water)_{*N*} clusters and to aid the estimation of the number of the water molecules explicitly hydrogen-bonded to a serine molecule in water, a MD simulation was carried out by using the Sander module in the AMBER9 suite of programs.³⁴ The AMBER *ff99* force field³⁴ based on molecular mechanics and TIP3P³⁴ water model were used in the simulation. An octagonal box with 21 serine molecules

and 1001 water molecules, corresponding to the 1 M experimental concentration, was used in the simulation. Briefly, the initial configuration was relaxed by applying 500 steps of steepest descent algorithm, followed by 500 steps of conjugate gradient algorithm to remove any bad contacts. To obtain the final configuration, the system was first heated from 0 to 298 K in 100 ps and was then equilibrated for 300 ps to ensure that the equilibrium was reached completely under NVT condition. Finally, a 7 ns production MD simulation was performed under NPT conditions ($T = 298$ K, $P = 1$ atm) with a time step of 2 fs. The long-range electrostatic interactions were treated with the particle mesh Ewald summation method,^{36,37} and the SHAKE algorithm³⁸ was used to constrain all covalent bonds involving the hydrogen atoms. For the non-covalent interactions, a 7 Å cutoff was introduced.

3.2.2.2 DFT calculations

All final geometry optimizations, harmonic frequency calculations, and the VA and VCD intensity predictions were performed at the B3LYP/6-311++G(d,p) level of theory, using the Gaussian 03 program package.³⁹ The B3LYP^{40,41} hybrid functional has been widely used in describing strong hydrogen-bonded complexes.⁴²⁻⁴⁴ Its reliability in predicting VCD intensities has also been well documented.⁴⁵⁻⁴⁸ The sensitivity of hydrogen-bonded systems to the basis set choice had been discussed before.^{49,50} The 6-311++G(d,p) basis set was chosen for its ability to successfully characterize hydrogen-bonded systems^{51,52} and to provide structures, and VA and VCD signatures in good agreement with the experimental data for this type of molecules and complexes.^{50,53-55} The tightest convergence criteria were used in the geometry optimizations to capture the small differences in bond length. To confirm that the optimized geometries were

true minima, their harmonic frequency calculations were checked to be without any imaginary frequencies. The predicted harmony frequencies were not scaled. To simulate the VA and VCD spectra, a Lorentzian line shape with a half width at half maximum of 10 cm^{-1} was used. To account for the water solvent, the VA and VCD spectra have also been simulated using the PCM^{31,32} as implemented in Gaussian 03. Within this model, the water solvent was treated as a continuum dielectric environment and a permittivity value of $\epsilon_0 = 78.390$ was used. The solution VA and VCD spectra have also been further simulated with the explicit hydrogen-bonding considerations described below.

3.3 Results and Discussions

3.3.1 Experimental VA and VCD spectra

To estimate the degree of self-aggregation of *L*-serine in water in the concentration range relevant to the current study, the concentration dependence of the VA spectra in water was measured first. The VA spectra in the frequency region from 1000 to 1450 cm^{-1} with eight different concentrations ranging from 0.1 M to the saturated solution are shown in Figure 3.1. Because of the strong H_2O absorption at $\sim 1600 \text{ cm}^{-1}$, the useful region is $1000\text{-}1450 \text{ cm}^{-1}$ with H_2O as a solvent. No noticeable band shifts or new bands have been observed, and the intensities of peaks increase linearly with increasing concentration. This suggests that no severe self-aggregation occurs in the concentration range used and additionally the dominant conformations have not changed. To further verify this conclusion, the VCD spectra at the three representative concentrations of 1.0 , 2.0 , and 3.0 M were measured and are provided in Figure

3.2. Again, the VCD spectra at the three concentrations appear to be very similar, further supporting the VA conclusion.

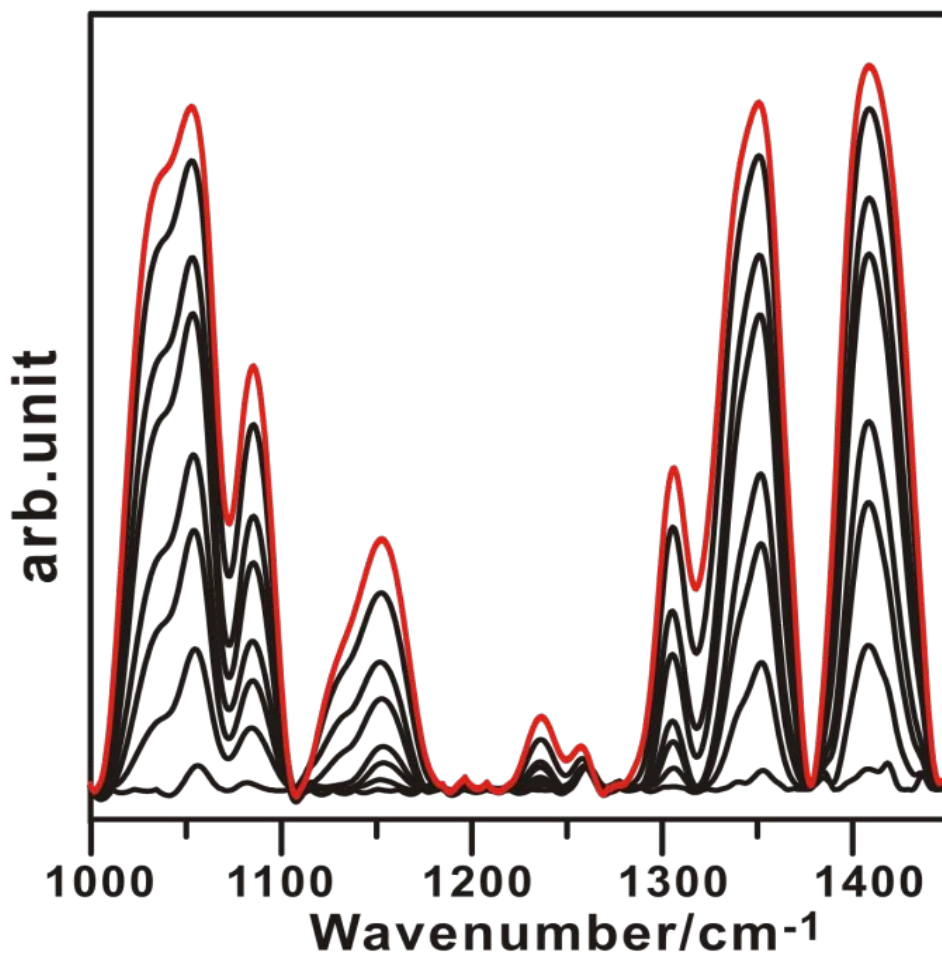


Figure 3.1 The experimental VA spectra of serine in water at a number of different concentrations between 0.1 M and saturation with an 0.5 M interval. The top (red, color online) line is the saturated solution.

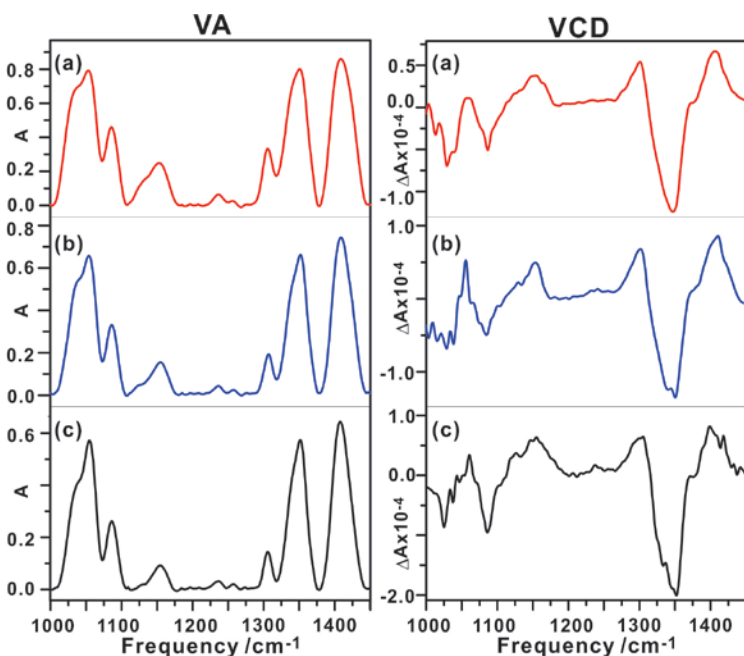


Figure 3.2 The experimental VA and VCD spectra of *L*-serine in water at three different concentrations (a) 3.0 M, (b) 2.0 M, and (c) 1.0 M.

While a naturally occurring amino acid exists mostly in its neutral form ($\text{H}_2\text{N}-\text{CHR}-\text{COOH}$) in the gas phase and in a non polar solvent, it exists primarily as ionic species in water and undergoes dissociation equilibria based on the acid dissociation constants of the amino and carboxylic acid functional groups. Such equilibria can be shifted by varying the pH of the solution. In the strongly acidic or basic aqueous solutions, the protonated or deprotonated forms can be expected to dominate, respectively, whereas zwitterions ($+\text{H}_3\text{N}-\text{CHR}-\text{COO}^-$) are typically the most abundant species in water around a neutral pH and in crystals. The experimental dissociation constants, i.e. pKa of serine, are 2.21 and 9.15,⁵⁶ corresponding to the dissociation of the COOH group and NH_3^+ group, respectively. One would therefore expect

that the protonated and the deprotonated species to become dominant at the pH of 1.0 and 13.0, respectively, whereas zwitterions are the dominant species at a pH value close to 7.

The VA and VCD measurements in H₂O at the pH values of 1.0 and 13.0 are provided in Figure 3.3, together with the corresponding measurements at the neutral pH. There are a number of noticeable differences in the VA and VCD spectra at different pH values. In the 1300-1450 cm⁻¹ region, the dominant VA bands are quite similar in all three pHs. In the 1200-1300 cm⁻¹ region, one most obvious difference in the VA spectra is the appearance of a new strong VA feature at ~1258 cm⁻¹ at pH=1 which is not there at either pH=13 or at the neutral pH. In the 1100-1200 cm⁻¹ region, the band at ~1154 cm⁻¹ in both pH=1 and at the neutral pH is replaced by two bands at ~1130 and 1178 cm⁻¹ in pH=13. Except the aforementioned differences at pH=1 and the neutral pH, the main spectral features in the 1000-1100 cm⁻¹ and 1300-1450 cm⁻¹ regions under these two pH values actually look quite similar in term of their relative intensities and their peak frequencies which correspond within 1 cm⁻¹ in the two spectra. Similar observations in these two regions could also be made in the corresponding VCD spectra. This suggests that the same zwitterionic species which exist at the neutral pH are at least partly responsible for these peaks at pH=1. At pH=13, the shape of the dominant feature in the 1000-1100 cm⁻¹ region changes noticeably from that at pH=1 or at the neutral pH. In the corresponding VCD spectra, one of the most noticeable difference is the disappearance of the negative VCD feature at ~1187 cm⁻¹ at pH=13.

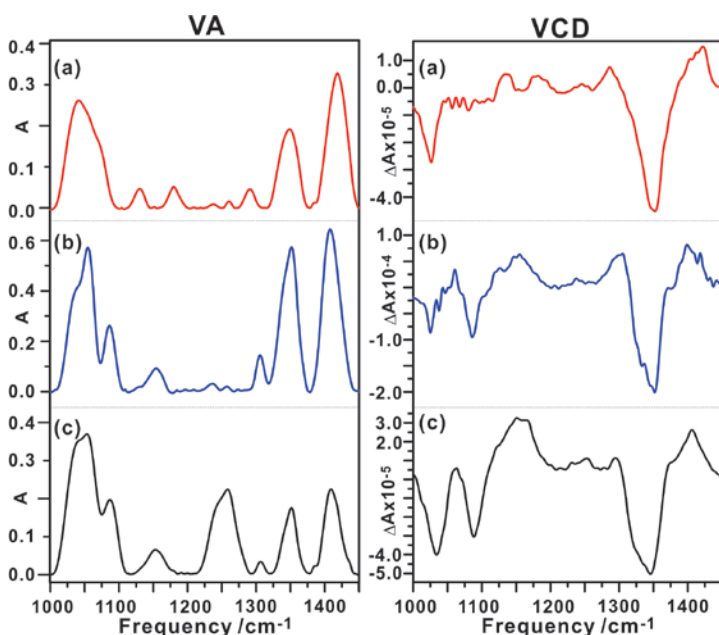


Figure 3.3 Comparisons of the experimental VA and VCD spectra of *L*-serine in H₂O at three different pH values of (a) 13.0, (b) 5.68 (denoted as ‘neutral’ in the text. See experimental section for details), and (c) 1.0.

The related VA and VCD measurements in D₂O at these three different pD values are summarized in Figure 3.4. In the 1550-1800 cm⁻¹ region, the peak at 1620 cm⁻¹ in the neutral D₂O measurement could be assigned to the asymmetric stretch of CO₂⁻, i.e. $\nu_{as}(\text{CO}_2^-)$, of the serine zwitterions, whereas the peak at 1579 cm⁻¹ at pH 13 has been assigned to $\nu_{as}(\text{CO}_2^-)$ of the deprotonated serine ionic species. There are two VA bands in this region for the pH=1 solution. One at 1731 cm⁻¹ is clearly the carbonyl stretch of COOD, while the other one at exactly the same frequency as in the neutral pH could be confidently assigned to $\nu_{as}(\text{CO}_2^-)$. The above VA assignment indicates that the deprotonated and zwitterionic species are the only dominant species at pH=13 and at neutral pH, respectively, whereas both protonated and zwitterionic

species coexist at pH=1. This corroborates the conclusion made with the H₂O measurements discussed above. Using the semi-empirical program SPARC,⁵⁷ a mixture of about 11% zwitterionic and 89% protonated serine species was predicted at pH=1, further supporting the above experimental conclusion.

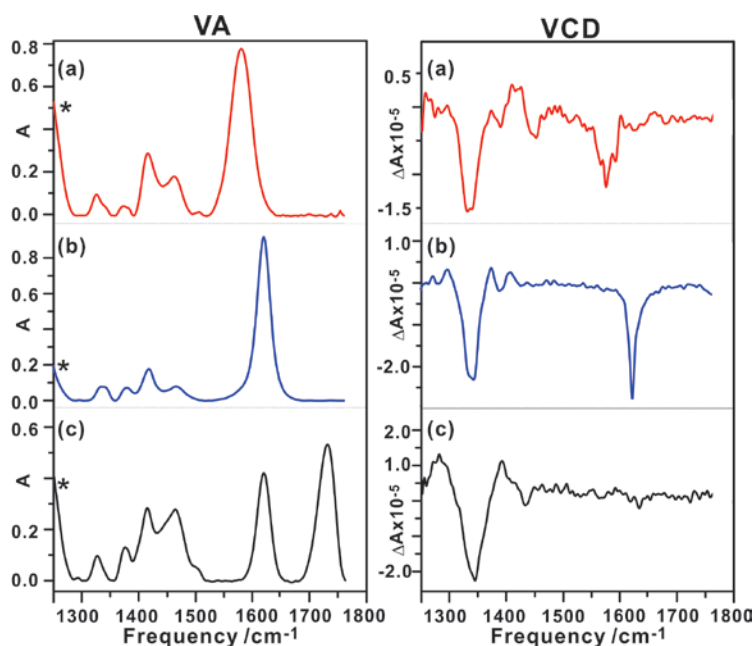


Figure 3.4 Comparisons of the experimental VA and VCD spectra of *L*-serine in D₂O at three different pD values of (a) 13.0, (b) 5.68, and (c) 1.0. * is due to the strong D₂O bending band.

The detailed assignments of the VA bands in the frequency region from 1000-1500 cm⁻¹ in H₂O and 1200-1500 cm⁻¹ in D₂O are less obvious. This is the region where the bending, scissoring, wagging, rocking modes of the CH, CH₂, NH₂ and NH₃⁺ groups are expected, as well as those related to the skeleton modes. Although some empirical assignments can be achieved tentatively by comparing to the molecules with the same functional groups, there is substantial

room for alternative assignments because it is very difficult to foresee the effects due to the conformational flexibility and the water solvent.

It is essential to apply theoretical modeling to unravel the conformational complexity and the effects of water on the observed VA and VCD spectra in order to conclusively identify the dominant species and their conformations in water. In particular, the VCD features are highly sensitive to conformational changes and hydrogen-bonding with water.²⁷⁻³⁰ The assignments of the dominant species, VA bands, and dominant conformations will thus be discussed below in the context of the VA and VCD simulations.

3.3.2 Simulations of the VA and VCD spectra of the monomeric conformers of the neutral, zwitterionic, protonated and deprotonated serine

In the present work, the geometry optimization of the *L*-serine neutral monomer was carried out at the B3LYP/6-311++G(d,p) level with the starting geometries taken from Ref. 4. The twelve lowest energy conformers of the serine monomer were obtained and are shown in Figure S1 in the supplementary material, together with the Boltzmann populations based on their relative Gibbs free energies at 298 K. The corresponding VA and VCD spectra of the four most stable conformers are provided in Figure 3.5. Although it is difficult to discount the contributions of the neutral serine conformers based on the comparison of the experimental and theoretical VA spectra, the calculated VCD features of these most stable conformers, with an overall population of ~80%, differ significantly from the experimental ones under the three different pH conditions. Clearly, the neutral serine monomers are not the dominant species in water under the experimental conditions considered here. This is in contrast to serine trapped

in the cold Ar-matrix where the experimental VA spectrum was reported to be well reproduced with several lowest energy neutral serine conformers at the B3LYP/6-31++G(d,p) level.¹⁰ Indeed, based on the empirical Ka calculations and the tentative VA spectra assignments discussed above, the protonated, zwitterionic, and deprotonated forms are expected to be the dominant species in water with a pH value of 1, 6 and 13, respectively.

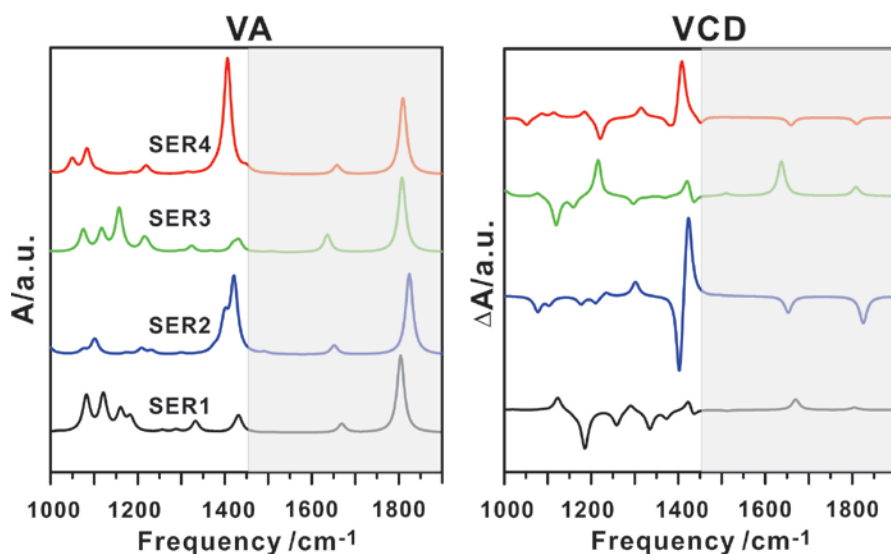


Figure 3.5 Simulated VA and VCD spectra of the four most stable neutral serine conformers at the B3LYP/6-311++G(d,p) level. The relevant wavenumber regions to the experimental data are left unshaded.

In the following, we will discuss the theoretical VA and VCD spectra of the lowest energy serine conformers of the three ionic species mentioned above, together with the corresponding species with deuterium substitution at the COOH, OH and NH₂ or NH₃⁺ group. The calculated results were compared with the corresponding experimental data in H₂O and D₂O to extract information about the most important serine conformers under each pH condition. We will

discuss the results in the following order from the neutral, to the basic, and finally to the acidic condition.

The optimized geometries of the four lowest energy conformers of the zwitterionic, deprotonated, and protonated forms of the serine monomer are shown in Figure 6, together with their Boltzmann population factors calculated based on their relative Gibbs free energies. The preferred site for deprotonation in the standard amino acids is typically the carboxyl group, although a recent theoretical calculation proposed that the most acidic site of cysteine is at the thio group.⁵⁸ In the four most stable protonated conformers, the amino group is protonated, as expected for a standard amino acid.⁵⁹ The important intermolecular bond distances are also indicated in the Figure 3.6.

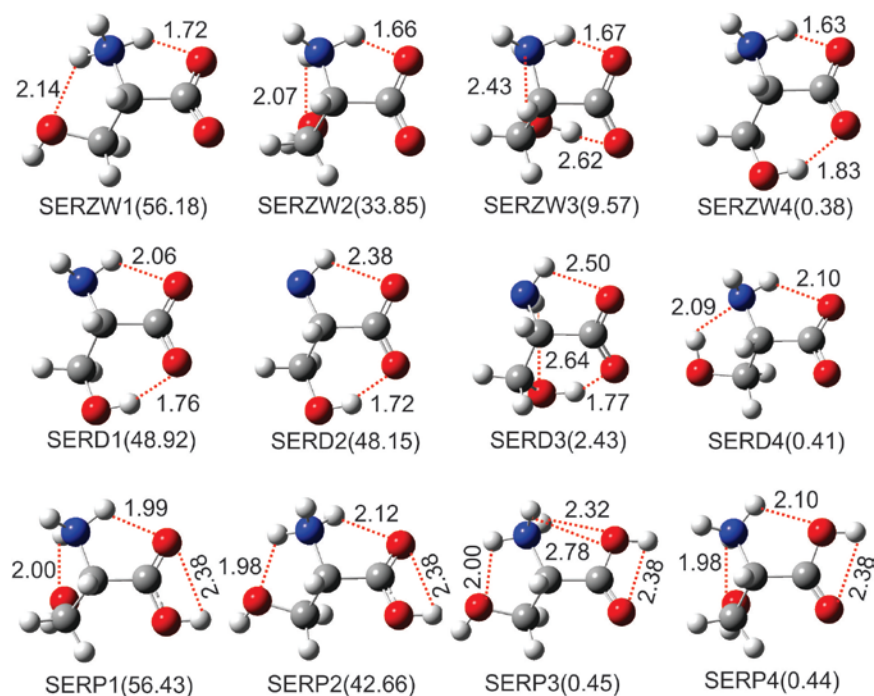


Figure 3.6 Optimized geometries of the four lowest energy conformers of the zwitterionic, deprotonated, and protonated monomeric serine conformers at the B3LYP/6-311++G(d,p) level

and the numbers in the parenthesis are the percentage populations at room temperature for each species separately based on the relative Gibbs free energies. The intermolecular hydrogen-bonding and secondary hydrogen-bonding bond lengths are indicated. In the latter cases, the H...O bond lengths are larger than $\sim 2 \text{ \AA}$ and shorter than 3 \AA .

The predicted VA and VCD spectra of the four most stable conformers of the zwitterionic form of serine are depicted in Figure 3.7(a). The initial inspection based on the VA spectra suggested that SERZW1 provides the best agreement with the experimental data, although SERZW2 and 3 also show some resemblance to the experimental data. Based on the simulated VA spectrum of SERZW1, the experimental spectrum from the $1000\text{-}1450 \text{ cm}^{-1}$ could be assigned. The three overlapped experimental peaks at 1038 , 1054 , and 1086 cm^{-1} could be assigned to the C-N stretching with some contribution for the O-H bending, the C-O stretching, and a mixture of N-H and C-H rocking modes, respectively, based on the GaussView visualization. The experimental band at 1154 cm^{-1} was tentatively assigned to a mixture of C-H, O-H and N-H rocking modes. Finally, the three peaks at 1306 , 1352 and 1408 cm^{-1} in the higher frequency end of the spectrum could be assigned to the modes dominated by the CH bending, N-H bending, and a mixture of C-H and N-H bending, respectively. Although at a first glance, the theoretical VCD spectrum of SERZW1 shows the dominant VCD features in reasonable agreement with the experimental data, some discrepancies in the peak frequencies of the VA and VCD spectra were noted. This point will be further discussed in the implicit and explicit solvation section below.

The simulated VA and VCD spectra of the deuterium zwitterionic serine conformers are provided in Figure 3.7(b). The strong experimental band at 1620 cm^{-1} could be unambiguously assigned to the asymmetric stretching of CO_2^- . The experimental VA and VCD features for this band were well reproduced theoretically. On the other hand, neither the multiple VA peaks observed experimentally in the $1250\text{-}1550\text{ cm}^{-1}$ region nor the corresponding strong VCD features were as well reproduced theoretically. The possible cause for such discrepancies is likely to be the hydrogen-bonding interactions between serine and water molecules.

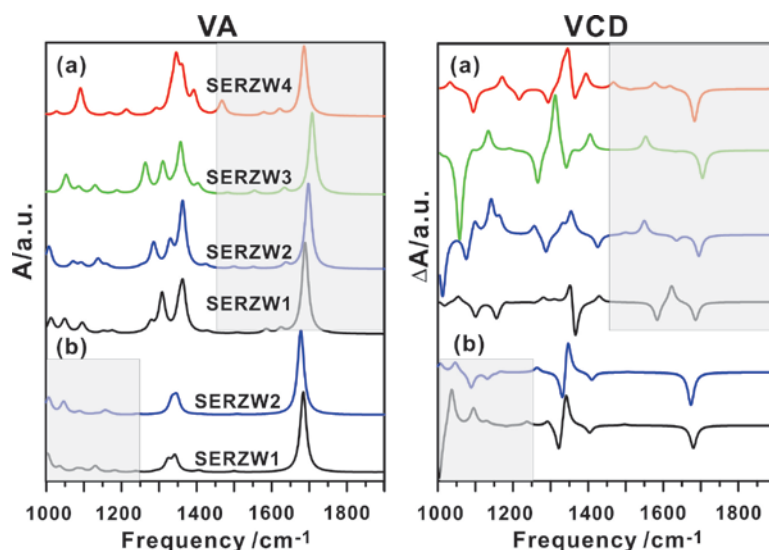


Figure 3.7 Simulated VA and VCD spectra of (a) the four most stable zwitterionic serine and of (b) two most stable deuterated zwitterionic serine conformers at the B3LYP/6-311++G(d,p) level. See text for the discussions on the deuterated species. The relevant wavenumber regions to the experimental data are left unshaded.

To understand the VA and VCD spectra at pH 13, the VA and VCD spectra of the four most stable deprotonated serine conformers were simulated and are depicted in Figure 3.8(a).

Based on the VA spectrum of SERD1, the severely overlapped bands at 1041 and 1072 cm^{-1} in the experimental VA spectrum could be assigned to a mixture of the C-H and N-H rocking modes, and the C-O stretching mode, respectively. The band at 1131 cm^{-1} was tentatively assigned to the C-N stretching mode, and the band at 1178 cm^{-1} to a mixture of C-H bending and NH_2 twisting mode together with a little bit of O-H bending. Only two bands were predicted for SERD1 in the 1000-1100 cm^{-1} region versus three for SERZW1, consistent with the fact that the third VA peak at 1086 cm^{-1} at pH neutral was not observed experimentally at pH=13. The difference observed in the 1100-1200 cm^{-1} region at pH=13 and neutral was also well captured by the simulations. The three peaks at the higher wavenumber of the spectrum have similar VA assignments as for SERZW1. The corresponding complex VCD features in the same frequency region were well reproduced theoretically, whereas the VCD features at the lower wavenumber region were not well captured at all.

Both the deuterated forms of SERD1 and SERD2 show similar VA and VCD spectral features (see Figure 3.8(b)) that resemble the experimental ones in D_2O closely. The strong VA band at 1578 cm^{-1} could be unambiguously assigned to the asymmetric stretching band of CO_2^- based on the VA prediction. The theoretical predictions also captured the experimentally observed red shift of $\sim 42 \text{ cm}^{-1}$ going from the neutral to pH 13 nicely, with a theoretical red shift of $\sim 73 \text{ cm}^{-1}$ (unscaled). Furthermore, the negative VCD feature at this wavenumber was well reproduced by the theoretical prediction. Finally, the strongly negative VCD band at 1343 cm^{-1} observed experimentally was also captured theoretically.

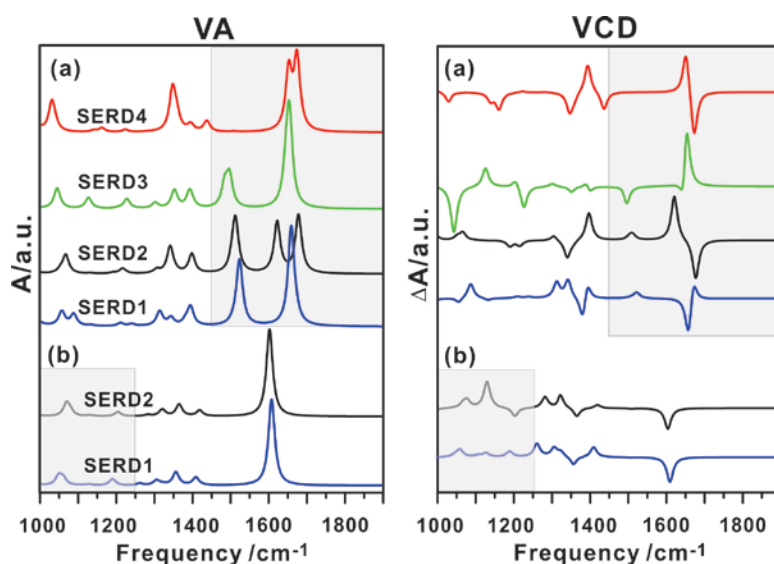


Figure 3.8 Simulated VA and VCD spectra of (a) the four most stable deprotonated serine and of (b) two most stable deuterated deprotonated serine conformers conformers at the B3LYP/6-311++G(d,p) level. See text for the discussions on the deuterated species. The relevant wavenumber regions to the experimental data are left unshaded.

As already discussed in Section 3.1, the experimental VA and VCD spectra clearly indicate that the zwitterionic and protonated forms of serine coexist at pH=1. In Figure 3.9(a), the simulated VA and VCD spectra of the four most stable protonated serine conformers are depicted. Clearly, the extra experimental VA feature at pH=13 versus the neutral pH, with a peak frequency at 1258 and a shoulder frequency at 1244 cm^{-1} , was captured with both SERP1 and SERP2 conformers. Such features were not there with SERZW1 or SERZW2. They could be assigned to the O-H bending modes in COOH and in COH. For the deuterated species, the simulated VA and VCD spectra are given in Figure 3.9(b). The VA measurement in D₂O shows a well isolated peak at 1731 cm^{-1} . This could be assigned to the carbonyl stretch modes of COOD

in SERP1 and/or SERP2 which were predicted to be at essentially the same wavenumber. The experimental VA peak at 1620 cm^{-1} is due to the antisymmetric CO_2^- stretching, i.e. $\nu_{\text{as}}(\text{CO}_2^-)$, of the zwitterionic species, keeping in mind that the zwitterionic species coexists at this pH as discussed in Section 3.3.1. The experimentally observed red shift of 111 cm^{-1} from $\nu_{\text{as}}(\text{COOD})$ to $\nu_{\text{as}}(\text{CO}_2^-)$ was correctly predicted theoretically with a value of 110 cm^{-1} using SERP1 and SERZW1. At the same time, the weak-medium intensity VCD signals with opposite signs were predicted for these SERP1 and SERP2 conformers. If both conformers are similarly populated in solution, one would expect no VCD signal at this wavenumber. This is exactly what was observed experimentally. Furthermore, the intense trisignate (+++) VCD feature at 1343 cm^{-1} could be reproduced by SERP1.

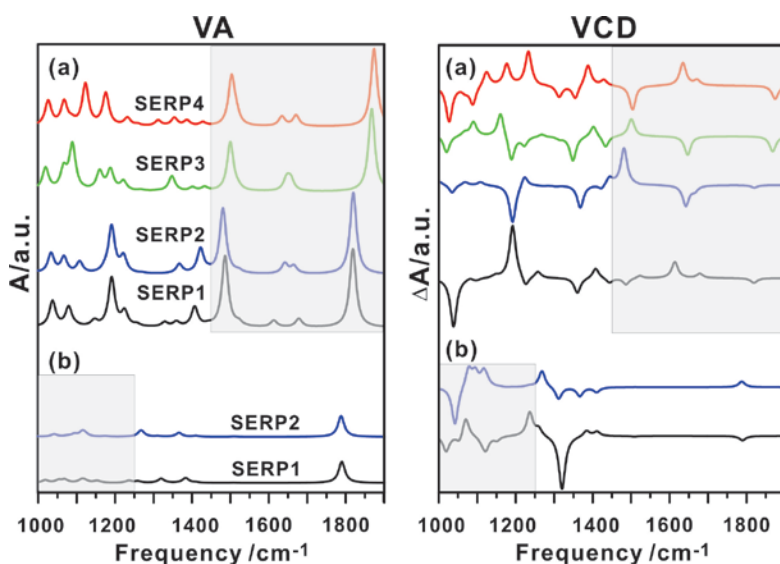


Figure 3.9 Simulated VA and VCD spectra of (a) the four most stable protonated serine and of (b) two most stable deuterated protonated serine conformers conformers at the B3LYP/6-

311++G(d,p) level. See text for the discussions on the deuterated species. The relevant wavenumber regions to the experimental data are left unshaded.

The above discussions showed that one can extract information about the most important conformers of the zwitterionic, deprotonated, and protonated species of serine under the three different pH conditions, based on the gas phase calculations of these species. That being said, it is noted that in some cases, the agreements between experimental and theoretical data are only marginal. It is well known that solvent can have severe effects on the experimental VA and VCD spectra. In particular, the solute induced chirality effects on solvent have been demonstrated in a number of molecular systems.^{22, 27-30} It is therefore desirable to include water in the spectral simulation.

One way to accomplish this is to use the continuum solvent models, such as PCM. On the other hand, the explicit hydrogen bonding with water molecules have been showed to be important in reproducing the experimental VA and VCD data and consequently in extracting important information about the conformations of the dominant species in solution. Therefore in the following, we will compare the results using both approaches and discuss their comparisons with the experimental data both in H₂O and D₂O solutions.

3.3.3 Explicit and continuum solvation models of the zwitterionic, deprotonated, and protonated serine with water

The RDFs obtained from the MD simulations are plotted in Figure S2 in the Supplementary Material, together with the atom labeling, to provide some general information

about the number of water molecules directly hydrogen-bonded to serine. For example, the RDF $g_{N1Ow}(r)$ provides information about the distribution of the oxygen atom of water from the selected origin, i.e. the N atom of serine, as a function of the distance, r , between them. The first maximum of $g_{N1Ow}(r)$ appears at 2.85 Å, and the integration to the next minimum gives a value of 3.16, corresponding to three water molecules in the first shell surrounding N of serine. Similarly, there are about 2.59 and 2.75 waters surrounding O2 and O3 (see Figure S2) of serine, the other two hydrogen-bonding sites of serine. A closer look at the MD snap shots revealed that some water molecules surrounding N1, O2, and O3 are counted twice. Therefore based both on the MD RDF analysis and our chemical intuition, we decided to solvate each serine species with six water molecules.

The two most stable monomeric serine conformers of each species have a combined population of 90% to 97% in all three cases of interest. We therefore added six water molecules to these two most stable conformers in each category to build the serine- (water)₆ clusters. The possible starting geometries were generated by using the MD snap shots, by maximizing the formation of cyclic hydrogen-bonding rings, and by considering the hydrogen-bonding capability of each functional group in serine. The theoretical results reveal that the geometry of the serine core does change slightly upon solvation with water. The relative energies and Gibbs free energies of the six most stable zwitterionic, deprotonated, and protonated serine-(water)₆ clusters are summarized in Table 3.1, together with their percentage Boltzmann populations. The geometries of the five most stable clusters of the solvated zwitterionic, deprotonated, and protonated serine are depicted in Figure 3.10. In the following discussions, we used the comparison of the unique experimental and theoretical

spectral features to guide our assignments of the most important species in solution. The theoretical relative Gibbs free energies were utilized only as a rough guide since the DFT free energy values are typically only reliable to a few kJ/mol.

Table 3.1. The relative total energies ΔE (kcal/mol) and the relative Gibbs free energies ΔG (kcal/mol) of the zwitterionic, deprotonated, and protonated serine-(water)₆ clusters at the B3LYP/6-311++G(d,p) level of theory and their percentage Boltzmann distributions at room temperature.

System	ΔE	$B_f(\Delta E)$	ΔG	$B_f(\Delta G)$
6ZW1	0.12	44.04	0	50.03
6ZW2	2.16	1.38	0.35	27.55
6ZW3	0	54.26	0.60	18.05
6ZW4	3.06	0.31	1.52	3.81
6ZW5	5.04	0.01	2.80	0.44
6ZW6	6.47	~0	4.41	0.03
6DEP1	0.98	11.83	0	39.84
6DEP2	1.64	3.87	0.31	23.60
6DEP3	0.62	21.81	0.38	21.00
6DEP4	0	61.66	0.68	12.56
6DEP5	3.62	0.14	1.59	2.73

6DEP6	3.21	0.27	3.21	0.18
6PRO1	0.91	5.96	0	57.74
6PRO2	0.75	7.77	0.49	24.87
6PRO3	0	54.83	1.05	9.85
6PRO4	0.41	27.48	1.54	4.26
6PRO5	1.20	3.63	1.72	3.15
6PRO6	3.17	0.13	4.05	0.06

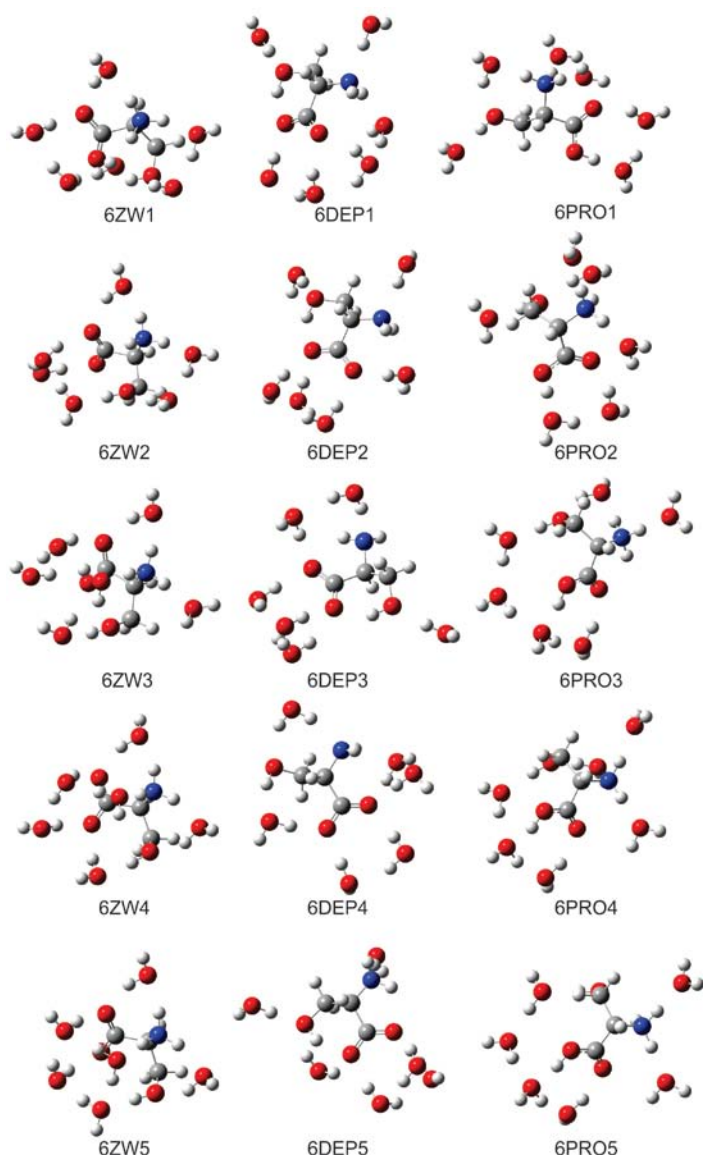


Figure 3.10 Optimized geometries of the five most stable zwitterionic, deprotonated, and protonated serine-(water)₆ clusters at the B3LYP/6-311++G(d,p) level.

For the pH neutral experiment, the simulated VA and VCD spectra of the five zwitterionic serine-(water)₆ conformers are provided in Figure 11(a), together with the experimental data in H₂O and the corresponding PCM simulations of SERZW1 and SERZW2 in H₂O for comparison. Considering the VA and in particular the VCD features, 6ZW5 provides the

best agreement with the experimental data. The more detailed assignments of the dominant bands are indicated by arrows in Figure 3.11(a). It is worth noting that the bands which have the same peak frequencies in the experimental VA and the corresponding VCD spectra could now be well correlated with those which also have the same peak frequencies in the simulated VA and VCD spectra. This was not exactly the case when the gas phase SERZW1 VA and VCD features were used to explain the observed spectra. So the inclusion of explicit serine-water interactions provides a better agreement between theory and experiment. The agreement between the experimental data with the PCM simulations of the two SERZW conformers, on the other hand, is quite poor.

The VA and VCD simulations for the five corresponding deuterated zwitterionic serine-(D₂O)₆ conformers are provided in Figure 3.11(b), together with the experimental data in D₂O and the corresponding PCM simulations of the deuterated SERZW1 and SERZW2 in D₂O for comparison. Again, 6ZW5 conformer provides the best agreement with the experimental data. Specifically, it captured most the dominant VA features and some important VCD features, although the experimental VCD feature centered at about 1337 cm⁻¹ was not so well reproduced. Although the simulated VCD spectrum of the deuterated SERZW2 in D₂O PCM gave slightly better agreement with the experimental data, it is clear that overall, the PCM simulated serine spectra in H₂O and D₂O do not provide good agreement with the experimental data. The explicit solvation, on the other hand, gives satisfactory agreement by using the normal and deuterated 6ZW5 conformers with H₂O and D₂O molecules, respectively.

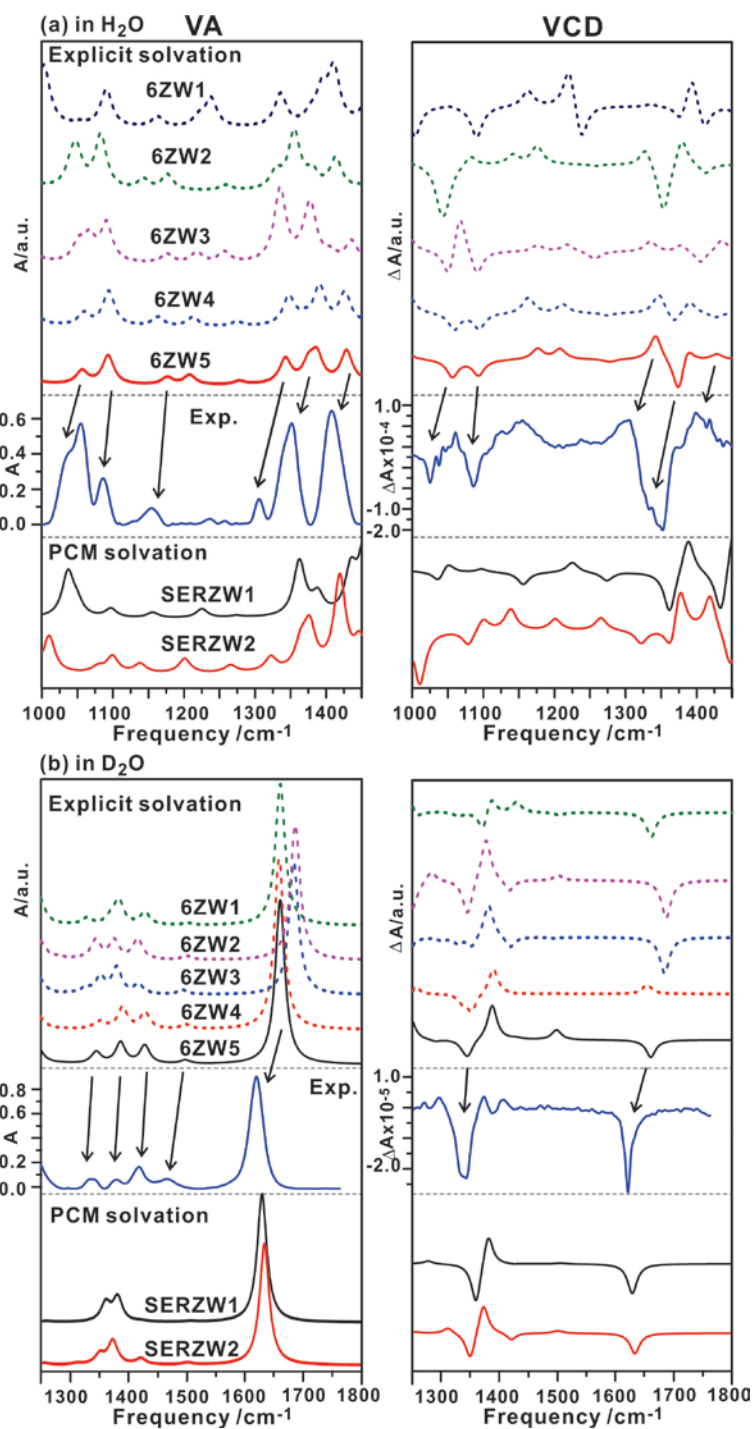


Figure 3.11 (a) Comparisons of the simulated VA (left) and VCD (right) spectra of the five most stable zwitterionic serine-(water)₆ conformers with the related experimental data in water at the neutral pH. The corresponding simulated VA and VCD of SERZW1 and SERZW2 in the PCM of water are depicted at the bottom. (b) Comparisons of the simulated VA (left) and VCD (right)

spectra of the five most stable deuterated zwitterionic serine-(D₂O)₆ conformers with the related experimental data in D₂O at the neutral pH. The corresponding simulated VA and VCD spectra of the deuterated SERZW1 and SERZW2 in the PCM of D₂O are depicted at the bottom.

For the experiment at pH 13, the simulated VA and VCD spectra of the four most stable deprotonated serine-(water)₆ conformers are provided in Figure 3.12(a), together with the experimental data in H₂O and the related PCM simulations of SERD1 and SERD2 for comparison. The related simulated VA and VCD spectra of the four most stable deprotonated deuterated serine-(D₂O)₆ conformers are provided in Figure 3.12(b), together with the experimental data in D₂O and the related PCM simulations for comparison. Taking into account both the normal and the deuterated species in the theory-experiment comparison, it is clear that 6DEP1 provides the best overall agreement with all the available experimental data. The assignments for the dominant spectral features are indicated by arrows in Figure 3.12. The PCM of DEP2 gives an ok agreement with the experiment, although slightly worse than 6DEP1. The explicitly solvated cluster 6DEP1 is the dominant species in solution which gives rise to the main observed spectral features.

For the experiment at pH 1, the simulated VA and VCD spectra of the four protonated serine-(water)₆ conformers are provided in Figure 3.13(a), together with the experimental data in H₂O and the related PCM simulations of SERP1 and SERP2 for comparison. Since the theoretical VA and VCD features do not differ drastically from one conformer to the next, we also present the population weighted VA and VCD spectra, labeled as 6PRO Av. As discussed in Sections 3.3.1 and 3.3.2, it is necessary to consider the zwitterionic species to explain the

observed spectra. An empirical weighting ratio of 50%:50% for 6ZW5 and 6PRO Av. was used to simulate the ZW+PRO VA and VCD spectra in Figure 3.13(a). With this approach, most of the experimental VA and VCD features could be explained and the corresponding assignments are indicated by arrows in the same figure. We would like to caution against taking this empirical 1:1 weighting ratio too literally since the spectra presented here are complicated with some severely overlapped lines. Even small frequency shifts in the simulated VA peaks can result in a noticeable change in the intensities of the overlapped peaks and therefore this estimated ratio. The PCM VA spectra of SERP1 and SERP2 fail to reproduce the strong extra VA feature observed experimentally at 1258 cm^{-1} when changing from the neutral pH to pH=1. At the same time, the simulated VCD spectra with PCM show poor correlation to the observed data.

The related simulated VA and VCD spectra of the four most stable protonated deuterated serine- $(\text{D}_2\text{O})_6$ conformers are provided in Figure 3.13(b), together with the experimental data in D_2O and the related PCM simulations for comparison. As with the normal species, the 6PRO Av and ZW+PRO VA and VCD spectra are also provided. Here an empirical ratio of 80%:20% for 6PRO Av versus 6ZW5 was used in order to reproduce the experimentally observed ratio between the VA bands at 1620 and 1731 cm^{-1} . Again, the ZW+PRO VA and VCD spectra captured all the essential features observed experimentally. The related assignments are indicated with the arrows in Figure 3.13(b). Considering both the normal and deuterated data, the explicitly solvated protonated and zwitterionic serine species with water has again provided an overall satisfactory explanation of the observed spectra. The implicit solvation with PCM, on the other hand, was inadequate for a detailed VA and VCD spectral assignment.

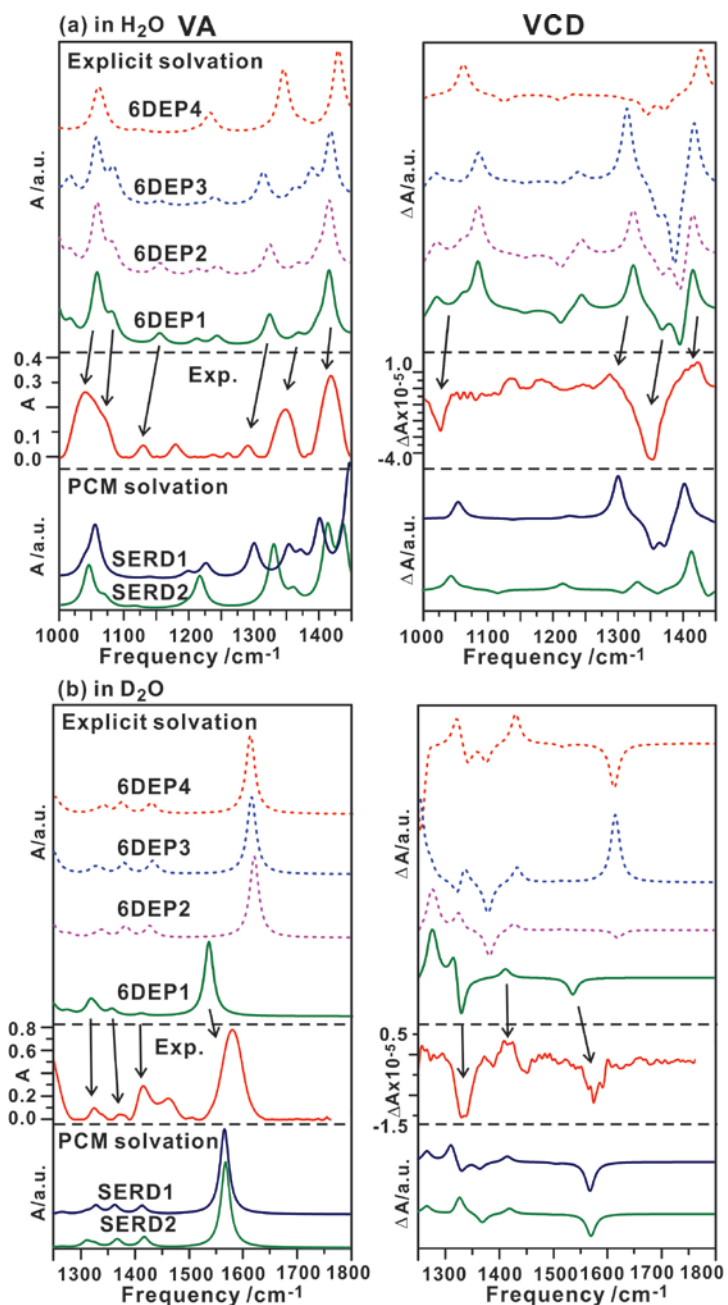


Figure 3.12 (a) Comparisons of the simulated VA (left) and VCD (right) spectra of the four most stable deprotonated serine-(water)₆ conformers with the related experimental data in water at pH=13. The corresponding simulated VA and VCD of SERD1 and SERD2 in the PCM of water are depicted at the bottom. (b) Comparisons of the simulated VA (left) and VCD (right) spectra of

the four most stable deuterated deprotonated serine-(D₂O)₆ conformers with the related experimental data in D₂O at pH=13. The corresponding simulated VA and VCD spectra of the deuterated SERD1 and SERD2 in the PCM of D₂O are depicted at the bottom.

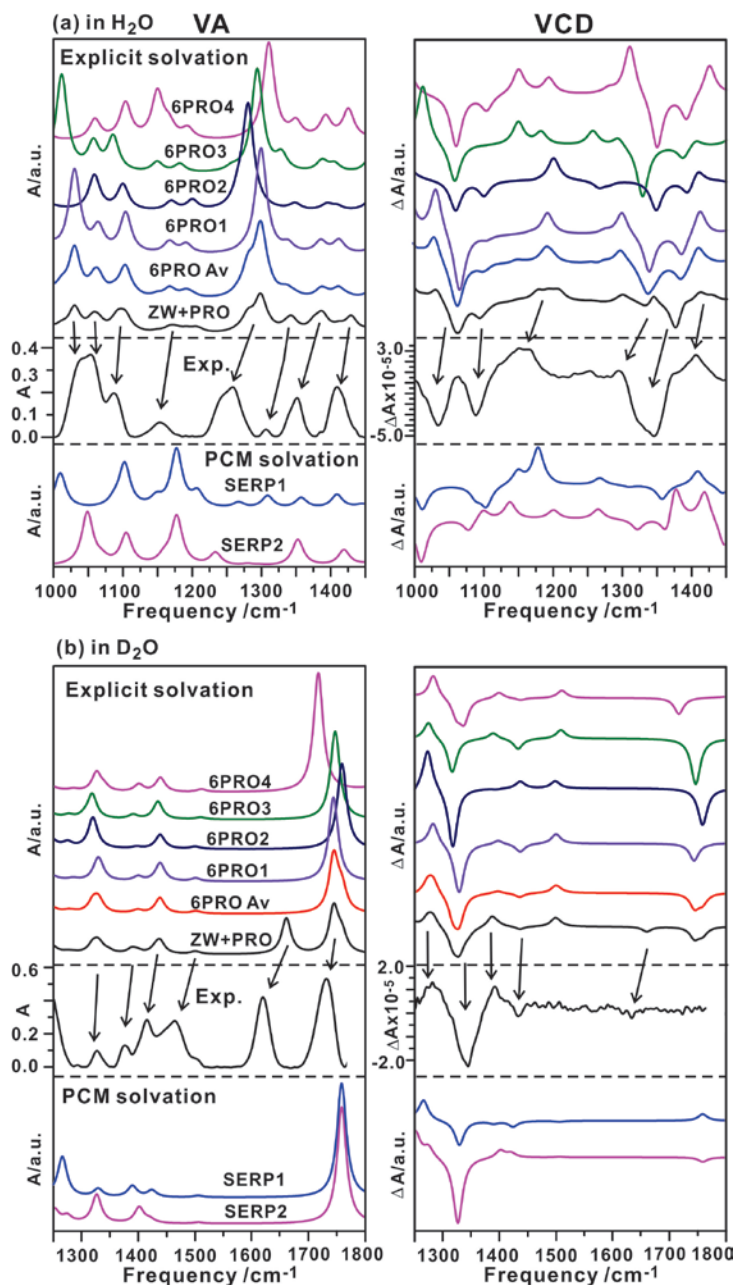


Figure 3.13 (a) Comparisons of the simulated VA (left) and VCD (right) spectra of the four most stable protonated serine-(water)₆ conformers with the related experimental data in water at

pH=1. The population weighted VA and VCD spectra of the protonated species and the simulated VA and VCD spectra with a combination of zwitterionic and protonated species are also provided. See text for the detailed discussions. The corresponding simulated VA and VCD of SERP1 and SERP2 in the PCM of water are depicted at the bottom. (b) Comparisons of the simulated VA (left) and VCD (right) spectra of the four most stable deuterated protonated serine-(D₂O)₆ conformers with the related experimental data in D₂O at pH=1. The population weighted VA and VCD spectra of the protonated species and the simulated VA and VCD spectra with a combination of zwitterionic and protonated species are also provided. The corresponding simulated VA and VCD spectra of the deuterated SERP1 and SERP2 in the PCM of D₂O are depicted at the bottom.

3.4 Conclusion

In this report, the dominant species and the conformational distributions of serine under three representative pHs, i.e., strongly acidic, near neutral, and strongly basic conditions, have been investigated using VA and VCD spectroscopy, complemented with *ab initio* calculations. It has been found that the dominant species are the deprotonated, zwitterionic, and a mixture of the protonated and zwitterionic forms of serine under strongly basic, near neutral, and strongly acidic conditions, respectively. Based on the gas phase simulations of one or two of the most stable conformers of each protonated, deprotonated and zwitterionic species, the experimental VA and VCD spectra could be largely interpreted, although some discrepancies have been noted. The availability of the experimental VA and VCD spectra in both H₂O and D₂O has been crucial for the identification of the dominant conformers. Inclusions of the water solvent by PCM and

by the explicit serine-water hydrogen-bonding interactions have been performed. While the former approach has not improved the agreement between the experimental and simulated VA and VCD spectra in general in the current study, the latter has been found to improve the agreement between the experiment and theory noticeably. This suggests that inclusion of explicit solvent-solute interactions is important for the interpretation of the solution VA and VCD spectra.

Supporting Information

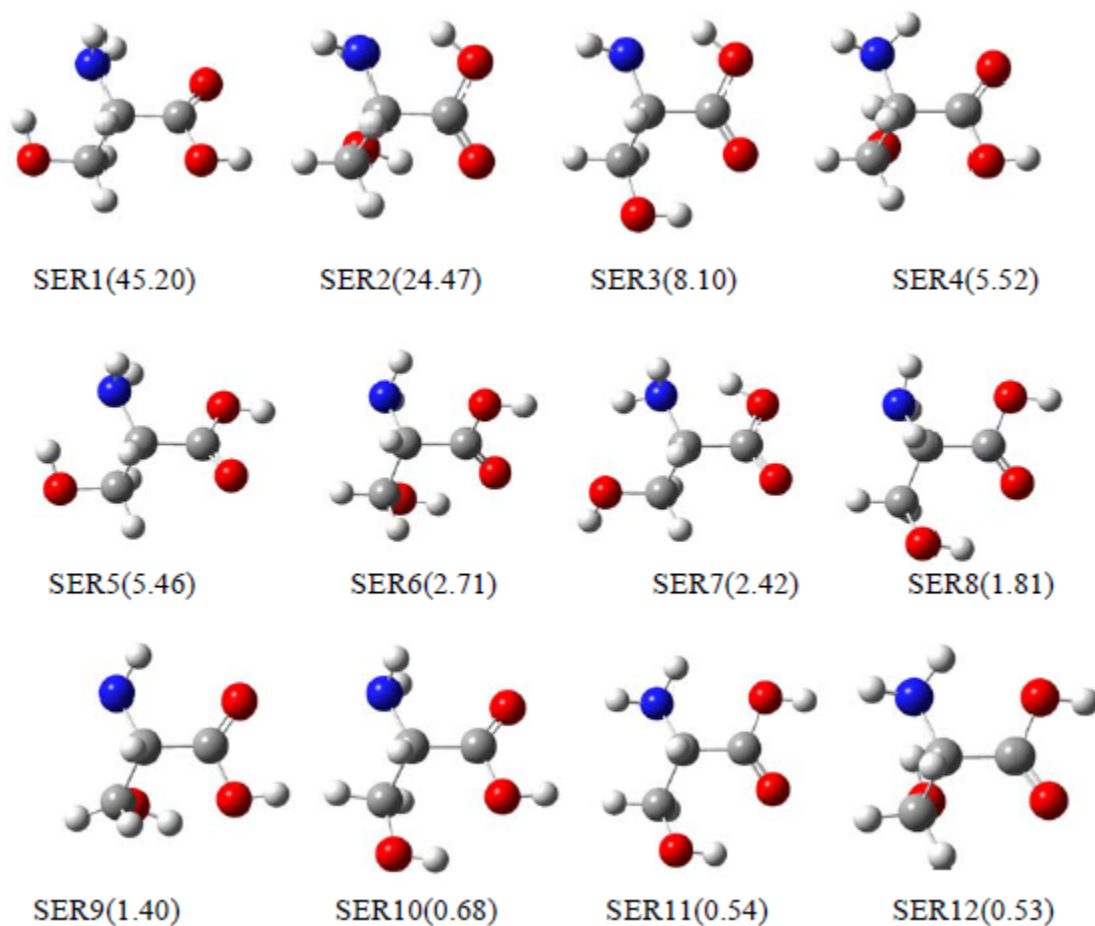


Figure S1. Optimized geometries of the twelve lowest energy conformers of the serine monomer at the B3LYP/6-311++G(d,p) level and the numbers in the parenthesis are the percentage populations based on the relative Gibbs free energies.

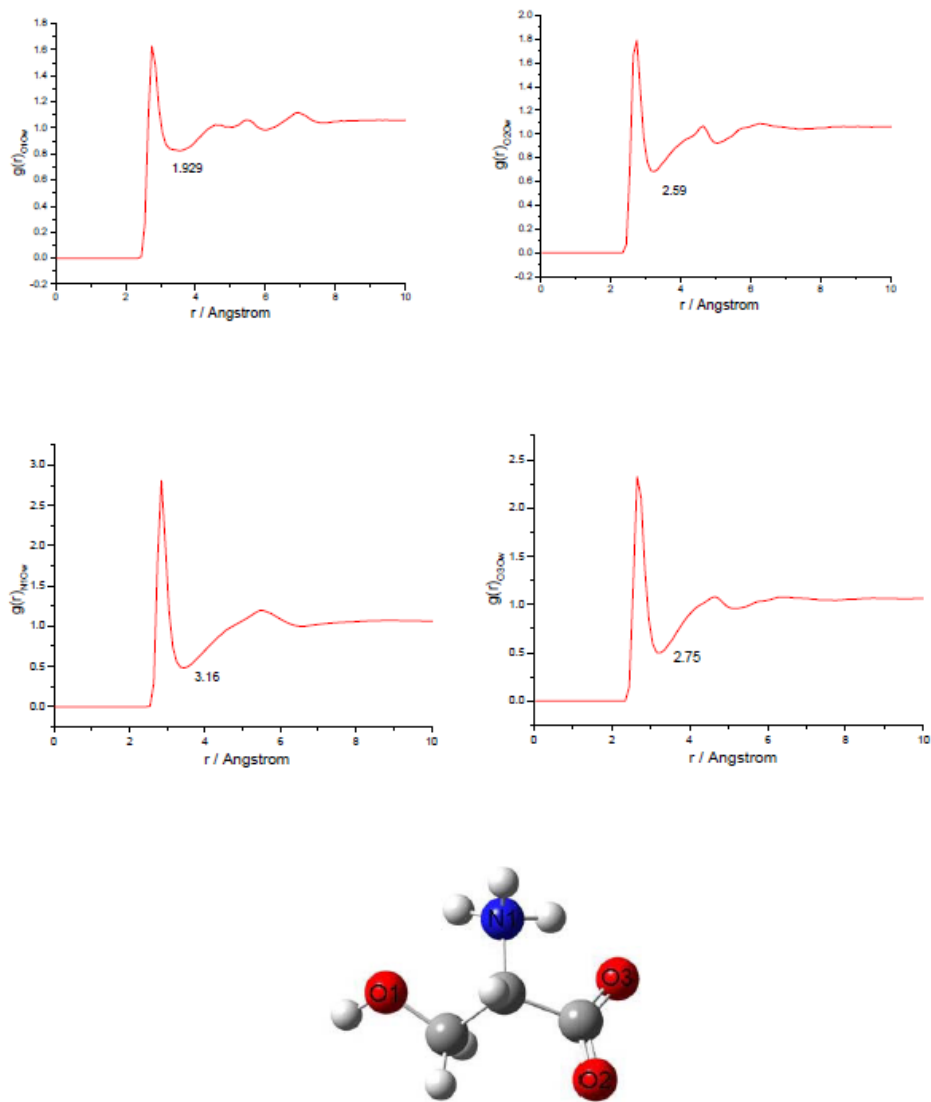


Figure S2. RDFs obtained from the MD simulation of the zwitterionic serine species in water. Ow and Hw are the oxygen and hydrogen atoms of water, respectively. The atom labeling of serine is give at the bottom. The numbers given in each figure are the water coordination numbers obtained by integration of the first peak out to the next minimum.

References:

1. P. Zhu, G. Yang, M. R. Poopari, Z. Bie, and Y. Xu, *Chem. Phys. Chem.*, 2012, **12**, 1272-1281.
2. G. Albrecht and R. B. Corey, *J. Am. Chem. Soc.*, 1939, **61**, 1087-1103.
3. F. R. Tortonda, J. L. Pascual-Ahuir, E. Silla, I. Tunonon, and F. J. Ramirez, *J. Chem. Phys.*, 1998, **109**, 592-602.
4. S. Gronert and R. A. J. O'Hair, *J. Am. Chem. Soc.* 1995, **117**, 2071-2081.
5. E. Tajkhorshid, K. J. Jalkanen, and S. Suhai, *J. Phys. Chem. B*, 1998, **102**, 5899-5913.
6. C. F. Correia, P. O. Balaj, D. Scuderi, P. Maitre, and G. Ohanessian, *J. Am. Chem. Soc.*, 2008, **130**, 3359-3370.
7. Z. Ji, R. Santamaria, and I. L. Garzón, *J. Phys. Chem. A*, 2010, **114**, 3591-3601.
8. C. H. Görbitz, *Acta Chem. Scand.*, 1990, **44**, 584-590.
9. T. M. Korter, R. Balu, M. B. Campbell, M. C. Beard, S. K. Gregurick, and E. J. Heilweil, *Chem. Phys. Lett.*, 2006, **418**, 65-70.
10. B. Lambie, R. Ramaekers, and G. Maes, *J. Phys. Chem. A*, 2004, **108**, 10426-10433.
11. F. J. Ramírez, I. Tuñón, and E. Silla, *Chem. Phys.*, 2004, **303**, 85-96.
12. I.-S. Jeon, D.-S. Ahn, S.-W. Park, S. Lee, B. Kim, *Int. J. Quant. Chem.*, 2005, **101**, 55-66.
13. R. Miao, C. Jin, G. Yang, J. Hong, C. Zhao, and L. Zhu, *J. Phys. Chem. A*, 2005, **109**, 2340-2349.
14. T. M. Korter, R. Balu, M. B. Campbell, M. C. Beard, S. K. Gregurick, and E. J. Heilweil, *Chem. Phys. Lett.*, 2006, **418**, 65-70.
15. W. M. Zuk, T. B. Freedman, and L. A. Nafie, *J. Phys. Chem.*, 1989, **93**, 1771-1779.
16. M. Diem, E. Photos, H. Khouri, and L.A. Nafie, *J. Am. Chem. Soc.*, 1979, **101**, 6829-6837.
17. S. C. Nanita and R. G. Cooks, *Angew. Chem. Int. Ed.*, 2006, **45**, 554-569.
18. G. A. Jeffrey and W. Saenger, 1991, *Hydrogen Bonding in Biological Structure*, Springer Verlag, Berlin.

19. P. Ball, 1999, *H₂O: A Biography of Water*, Weidenfeld & Nicolson, London.
20. M. Yves, 2007, *The Hydrogen Bond and the Water Molecule*, Elsevier, New York.
21. L. A. Nafie, R. K. Dukor and T. B. Freedman, *Handbook of Vibrational Spectroscopy*, ed. J. M. Chalmers and P. R. Griffiths, John Wiley & Sons, Chichester, UK, 2002, **1**, pp. 731–744.
22. G. Yang and Y. Xu, “Vibrational Circular Dichroism Spectroscopy of Chiral Molecules”, in *Top Curr. Chem., Volume: Electronic and Magnetic Properties of Chiral Molecules and Supramolecular Architectures*, Eds R. Naaman, D. N. Beratan, and D. H. Waldeck, Springer Verlag Berlin Heidelberg, 2011, **298**, 189-236.
23. T. A. Keiderling, *Curr. Opinion Chem. Bio.*, 2002, **6**, 682-688.
24. S. Pizzanelli, C. Forte, S. Monti, G. Zandomenoghi, A. Hagarman, T. J. Measey, R. Schweitzer Stenner, *J. Phys. Chem. B*, 2010, **114**, 3965-3978.
25. S. Yang and M. Cho, *J. Chem. Phys.*, 2009, **131**, 135102.
26. R. Schweitzer-Stenner, *J. Phys. Chem. B*, 2009, **113**, 2922-293.
27. M. Losada, H. Tran, and Y. Xu, *J. Chem. Phys.*, 2008, **128**, 014508.
28. M. Losada, P. Nguyen, and Y. Xu, *J. Phys. Chem. A* 2008, **112**, 5621-5627.
29. G. Yang and Y. Xu, *J. Chem. Phys.* 2009, **130**, 164506.
30. M. Losada and Y. Xu, *Phys. Chem. Chem. Phys.*, 2007, **9**, 3127-3135.
31. S. Miertus, E. Scrocco, J. Tomasi, *Chem. Phys.*, 1981, **55**, 117-129.
32. J. Tomasi, M. Persico, *Chem. Rev.*, 1994, **94**, 2027-2094.
33. X. L. Cao, R. K. Dukor and L. A. Nafie, *Theo. Chem. Account*, 2008, **119**, 69-79.
34. D. A. Case, T. A. Darden, T. E. Cheatham, C. L. Simmerling, J. Wang, R. E. Duke, R. Luo, K. M. Merz, D. A. Pearlman, M. Crowley, R. C. Walker, W. Zhang, B. Wang, S. Hayik, A. Roitberg, G. Seabra, K. F. Wong, F. Paesani, X. Wu, S. Brozell, V. Tsui, H. Gohlke, L. Yang, C. Tan, J. Mongan, V. Hornak, G. Cui, P. Beroza, D. H. Mathews, C. Schafmeister, W. S. Ross, P. A. Kollman, AMBER 9; University of California, San Francisco, CA, 2006.
35. W. L. Jorgensen and C. Jenson, *J. Comp. Chem.* 1998, **19**, 1179.
36. H. Q. Ding, N. Karasawa, and W. A. Goddard, *J. Chem. Phys.* 1992, **97**, 4309.

37. U. Essmann, L. Perera, M. L. Berkowitz, T. Darden, H. Lee, and L. G. Pedersen, *J. Chem. Phys.*, 1995, **103**, 8577-8593.
38. J. P. Ryckaert, G. Ciccotti, and H. J. C. Berendsen, *J. Comp. Phys.*, 1977, **23**, 237-341.
39. M. J. Frisch, G. W. Trucks, H. B. Schlegel, G. E. Scuseria, M. A. Robb, J. R. Cheeseman, J. Montgomery Jr., T. Vreven, K. N. Kudin, J. C. Burant, J. M. Millam, S. S. Iyengar, Tomasi, V. Barone, B. Mennucci, M. Cossi, G. Scalmani, N. Rega, G. A. Petersson, H. Nakatsuji, M. Hada, M. Ehara, K. Toyota, R. Fukuda, J. Hasegawa, M. Ishida, T. Nakajima, Y. Honda, O. Kitao, H. Nakai, M. Klene, X. Li, J. E. Knox, H. P. Hratchian, J. B. Cross, V. Bakken, C. Adamo, J. Jaramillo, R. Gomperts, R. E. Stratmann, O. Yazyev, A. J. Austin, R. Cammi, C. Pomelli, J. W. Ochterski, P. Y. Ayala, K. Morokuma, G. A. Voth, P. Salvador, J. J. Dannenberg, V. G. Zakrzewski, S. Dapprich, A. D. Daniels, M. C. Strain, O. Farkas, D. K. Malick, A. D. Rabuck, K. Raghavachari, J. B. Foresman, J. V. Ortiz, Q. Cui, A. G. Baboul, S. Clifford, J. Cioslowski, B. B. Stefanov, G. Liu, A. Liashenko, P. Piskorz, I. Komaromi, R. L. Martin, D. J. Fox, T. Keith, M. A. Al-Laham, C. Y. Peng, A. Nanayakkara, M. Challacombe, P. M. W. Gill, B. Johnson, W. Chen, M. W. Wong, C. Gonzalez and J. A. Pople, Gaussian 03, Revision E.01, Gaussian, Inc., Wallingford, CT, 2004.
40. A. D. Becke, *J. Chem. Phys.*, 1993, **98**, 5648-5652.
41. C. T. Lee, W. T. Yang, R. G. Parr, *Phys. Rev. B*, 1988, **37**, 785-789.
42. A. K. Chandra, S. Parveen, and T. Zeegers-Huyskens, *J. Phys. Chem. A*, 2007, **111**, 8884-8891.
43. J. N. Woodford, *J. Phys. Chem. A*, 2007, **111**, 8519-8530.
44. P. I. Dem'yanov, R. M. Gschwind, *Organometallics*, 2006, **25**, 5709-5723.
45. P. J. Stephens, F. J. Devlin, C. F. Chabalowski, and M. J. Frisch, *J. Phys. Chem.*, 1994, **98**, 11623-11627.
46. T. Kuppens, W. Herrebout, B. van der Veken, and P. Bultinck, *J. Phys. Chem. A*, 2006, **110**, 10191-10200.
47. L. Ducasse, F. Castet, A. Fritsch, I. Huc, and T. Buffeteau, *J. Phys. Chem. A*, 2007, **111**, 5092-5098.
48. T. Brotin, D. Cavagnat, J.-P. Dutasta, and T. Buffeteau, *J. Am. Chem. Soc.*, 2006, **128**, 5533-5540.
49. S. Scheiner, *Hydrogen Bonding: A Theoretical Perspective*, Oxford University Press: New York, 1997.

50. A. Karpfen, *Case studies in cooperativity in hydrogen-bonded clusters and polymers. In Molecular Interactions. From Van der Waals to Strongly Bound Complexes*, Ed. S. Scheiner, John Wiley & Sons: Chichester, UK, 1997; pp 265-296.
51. N. Borho and Y. Xu, *Angew. Chem.*, 2007, **119**, 2326-2329; *Angew. Chem. Int. Ed.*, 2007, **46**, 2276-2279.
52. Z. Su, N. Borho, and Y. Xu, *J. Am. Chem. Soc.*, 2006, **128**, 17126-17131.
53. W. L. Qian and S. Krimm, *J. Phys. Chem. A*, 2002, **106**, 6628-6636.
54. A. Kovacs, A. Szabo, D. Nemcsok, and I. Hargittai, *J. Phys. Chem. A*, 2002, **106**, 5671-5678.
55. B. Kirchner and M. Reiher, *J. Am. Chem. Soc.*, 2002, **124**, 6206-6215.
56. C. P. Woodbury, *Biochemistry for the Pharmaceutical Sciences*, Jones & Bartlett Learning. 2011.
57. L. A. Carreira, S. Hilal, and S. W. Karickhoff, "*Estimation of Chemical Reactivity Parameters and Physical Properties of Organic Molecules Using SPARC*", and Eds. P. Politzer and J. S. Murray *Theoretical and Computational Chemistry, Quantitative Treatment of Solute/Solvent Interactions*, Elsevier Publishers, 1994.
58. Z. Tian, A. Pawlow, J. C. Poutsma, and S. R. Kass, *J. Am. Chem. Soc.*, 2007, **129**, 5403-5407.
59. M. Noguera, L. Rodríguez-Santiago, M. Sodupe, and J. Bertran, *J. Mol. Struct. (Theo.)*, 2001, **537**, 307-318.

Chapter 4

Preliminary Results of the Conformational Analysis of Leucine in Water

4.1 Introduction

Leucine, $\text{HO(O)CCH(NH}_2\text{)CH}_2\text{CH(CH}_3\text{)}$, together with valine and isoleucine, are the three so-called branched-chain amino acids which play important roles in protein structure, metabolism and regulation.¹ In particular, leucine has the capacity for stimulating muscle protein synthesis and is now considered as the most important amino acid for maintaining and for stimulating the growth of skeletal muscle.² Because of its large bulky branched side chain, leucine exhibits hydrophobicity. For example, in proteins, leucine is largely excluded from aqueous environments but interacts well with other hydrophobic molecules. It is of considerable interest to compare the conformations and dominant species of leucine in water to those of serine in water. In this chapter, the preliminary study of the conformations of leucine in water under three different pH conditions is described. Similar strategy as described in Chapter 3 for serine was applied.

4.2 Experimental Methods

The same instrument used for the serine study was also used for the leucine study here. For the current measurements, a pair of BaF₂ windows (International Crystal Laboratories) with variable path lengths was used. *L*- (98%) and *D*-leucine (99%) were purchased from Sigma Aldrich and used without further purification. The doubly distilled water and D₂O (99.99%) from Sigma Aldrich were used as solvents. Leucine can exist in water as several different species, such as the protonated, deprotonated, and zwitterionic species by tuning the solution pH values. Three representative pH values of 1.0, 6.4, and 13 were selected. The pH or pD values of 1.0 and 13.0 were achieved by adding a highly concentrated 6 M HCl or DCl solution and NaOH or NaOD solution, respectively, whereas a pH of 6.4 was obtained experimentally when no strong acid or base was added. The last condition is referred to as “neutral” from now on. Due to the low solubility of leucine in water, VCD measurements could only be achieved reliably for the neutral condition in D₂O solution, whereas VA measurements were done in both H₂O and D₂O under three pH conditions. A path length of 50 μm and a concentration of ~ 0.15 M were used. The VCD measurements of *L*-leucine were corrected with the corresponding measurements of *D*-leucine under identical experimental conditions to minimize any VCD artefacts.³ For the VCD measurements, a collection time of 240 minutes and a 4 cm⁻¹ resolution were applied.

4.3 Computational Details

All final geometry optimizations, harmonic frequency calculations, and the VA and VCD intensity⁴ predictions were performed at the B3LYP/6-311++G(d,p) level of theory⁵, using the

Gaussian 03 program package.⁶ The tightest convergence criteria were used in the geometry optimizations to capture the small differences in bond length. To confirm that the optimized geometries were true minima, their harmonic frequency calculations were checked to be without any imaginary frequencies. The predicted harmonic frequencies were not scaled. To simulate the VA and VCD spectra, a Lorentzian line shape with a half width at half maximum of 10 cm^{-1} was used. To account for the water solvent, the VA and VCD spectra have also been simulated using the PCM as implemented in Gaussian 03. The water permittivity value of 78.390 was used.

4.4 Results and Discussions

4.4.1 Experimental VA and VCD spectra

Because leucine is a hydrophobic amino acid, the solubility is low in water. Moreover, because of the strong broad H_2O bending band at $\sim 1640\text{ cm}^{-1}$, the useful region is $1000\text{-}1450\text{ cm}^{-1}$ for the VA measurements with H_2O as a solvent. Even with the maximum concentration of $\sim 0.15\text{ M}$, the intensities of all VA peaks of interest are still too weak to perform reliable VCD measurements. As a result, no VCD spectra in H_2O were obtained. In order to detect the spectral features in the $1500\text{ to }1800\text{ cm}^{-1}$ region, experiments in D_2O were also performed.

Since leucine has a dissociation constant (pKa) value of 2.33 and 9.74,⁷ one may expect the deprotonated leucine at pH 13 and the protonated leucine at pH 1. The VA measurements in H_2O at three representative pHs are shown in Figure 4.1. The VA spectra of pH 1 and 13 are obviously different from the one under neutral condition. In Figure 4.2, the corresponding VA measurements in D_2O in the $1500\text{-}1800\text{ cm}^{-1}$ region are given.

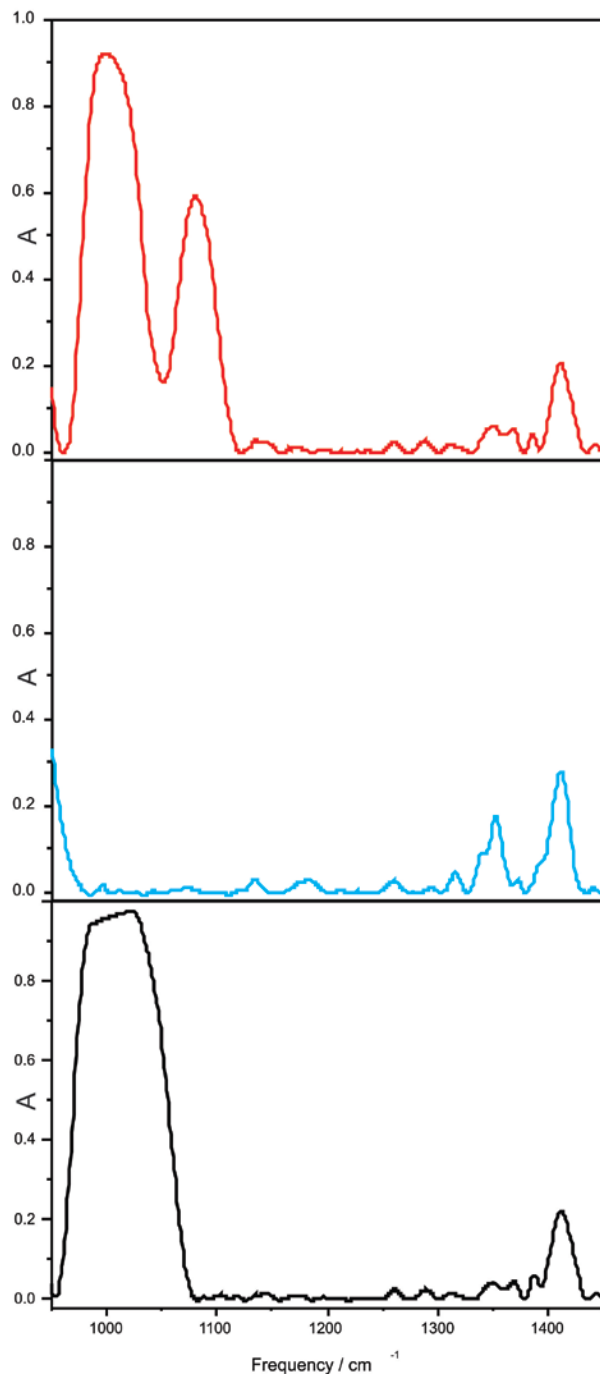


Figure 4.1 Comparisons of the experimental VA spectra of *L*-leucine in H₂O at three different pH values of 13.0, 6.4, and 1.0 from top to bottom.

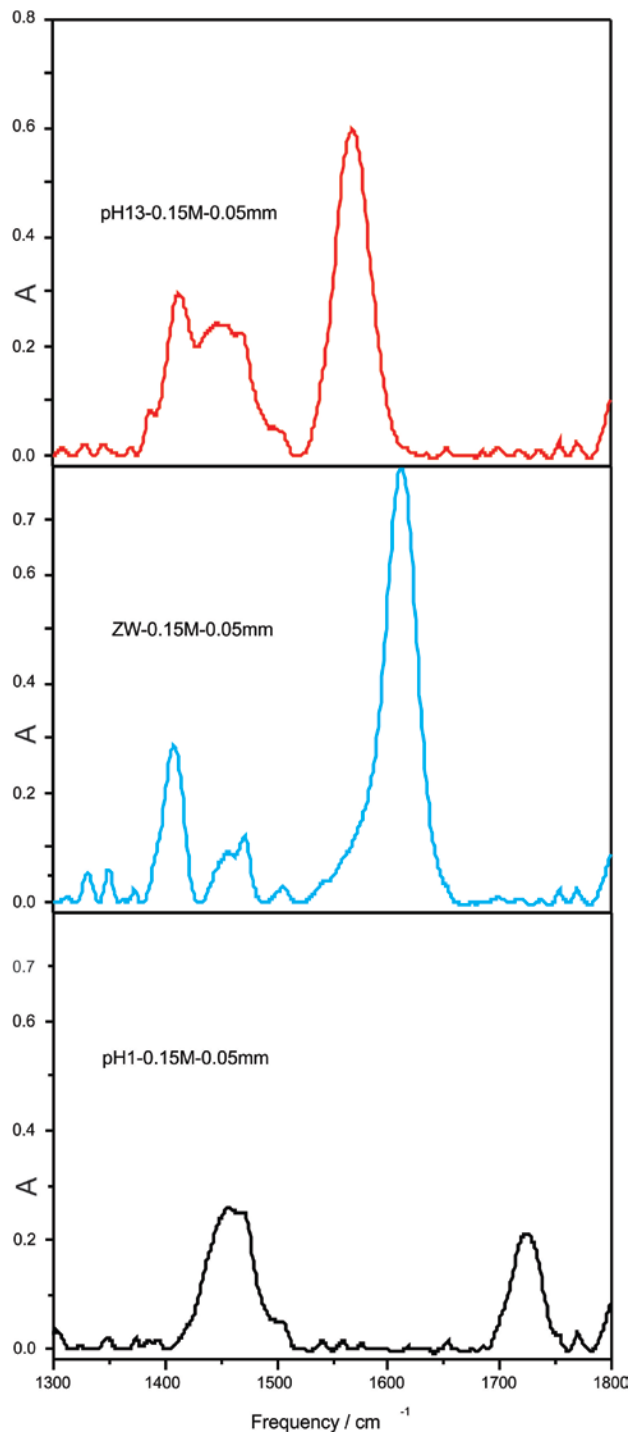


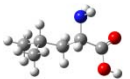
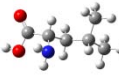
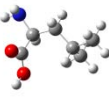
Figure 4.2 Comparisons of the experimental VA spectra of *L*-leucine in D₂O at three different pD values of 13.0, 6.4, and 1.0 from top to bottom.

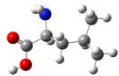
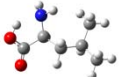
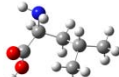
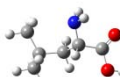
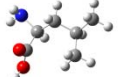
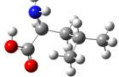
4.4.2 Comparison of the experimental and experimental VA and VCD spectra

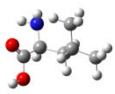
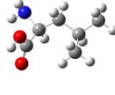
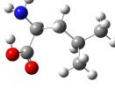
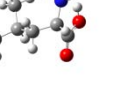
4.4.2.1 Conformers of neutral, protonated and deprotonated leucine in the gas phase

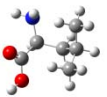
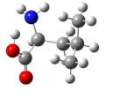
Emilio et al,⁸ reported a systematic search for the conformers of neutral leucine where 27 possible leucine structures were identified. I also carried out extensive search for possible neutral leucine structures with a lower basis set and obtained similar results as in Ref. 8. For the final results, B3LYP/6-311++G** was used for all the rest of calculations of leucine.^{9,10} In Table 4.1, a summary of the 27 possible neutral leucine structures identified is presented. It is well known that the preferred site for protonation in amino acids is typically the amino group.¹¹ The three most stable protonated conformers are shown in Figure 4.3, as well as the three most stable deprotonated conformers. Amino acids are well-known to exist as zwitterions in the solid state and in aqueous solution, although they tend to exist as neutral in the gas phase and the zwitterionic form may not even be stable in the gas phase. The optimized geometries of the three lowest energy conformers of the zwitterionic leucine monomer are given in Figure 4.3. These calculation results show that the intramolecular H-bonds play an important role in deciding the relative stability of conformers of leucine and its related ions. Higher energy conformers were also obtained for these three species, although they are much less stable than the three most stable ones presented here and are of little significance at room temperature. From the calculated results, one can see that the three lowest energy conformers of the three leucine species all contain the NH...O(=C) hydrogen bond. The hydrogen bond lengths in the protonated, deprotonated, and zwitterionic leucine conformers are also provided in Figure 4.3.

Table 4.1 Summary of 27 neutral leucine structures calculated

Name	structures	Population %	Energy G (hartree)	ΔG (kcal/mol)	ΔZPE (hartree)	ΔZPE (kcal/mol)	Rotational Constants	Dipole Moments
1		52.03609	-441.673409	0	0.192255	120.64172	2.70629 0.83490 0.78570	X= -0.1382 Y= -1.0457 Z= 0.4645
2		14.94282	-441.672231	0.73920626	0.192741	120.94666	2.86872 0.82473 0.75787	X= -3.9365 Y= 4.1703 Z= -0.1452
3		8.99696	-441.671752	1.039783339	0.192287	120.66219	2.72375 0.81614 0.79648	X= -0.2478 Y= -1.6544 Z= 0.0549
4		6.223263	-441.671404	1.258156666	0.192434	120.75408	2.17718 1.01867 0.91126	X= 0.3068 Y= -1.2017 Z= -0.6755
5		4.914051	-441.671181	1.398091297	0.192817	120.99476	2.36967 0.98857 0.87766	X= -0.9930 Y= 4.8321 Z= 1.2959
6		4.318376	-441.671059	1.474647464	0.192350	120.70120	2.18250 1.00399 0.92613	X= -0.2601 Y= 0.5400 Z= 1.4132

7		1.731196	-441.670196	2.016188213	0.192184	120.59728	2.74101 0.87796 0.72585	X= -0.0878 Y= -1.0309 Z= -0.7602
8		1.168661	-441.669825	2.248994259	0.192804	120.98644	2.82592 0.87436 0.72607	X= 4.1564 Y= 3.9377 Z= -0.0593
9		0.892053	-441.66957	2.409009197	0.192425	120.74871	2.32806 1.05126 0.93487	X= 0.1760 Y= -0.7722 Z= -0.9026
10		0.890165	-441.669568	2.410264216	0.192226	120.62392	2.75966 0.85491 0.74197	X= -0.2637 Y= 0.8747 Z= 1.2446
11		0.777305	-441.66944	2.49058544	0.192447	120.76221	2.79741 0.91616 0.79312	X= 0.0079 Y= -1.2584 Z= 0.0496
12		0.764243	-441.669424	2.500625593	0.192759	120.95812	2.77829 0.93176 0.77348	X= -4.5755 Y= 3.4493 Z= 0.5613
13		0.70663	-441.66935	2.5470613	0.192356	120.70527	2.33078 1.04100 0.85360	X= -0.4462 Y= -0.4787 Z= -1.0248
14		0.43641	-441.668895	2.832578149	0.193043	121.13608	2.44550 1.04202 0.92904	X= 2.5773 Y= 4.7700 Z= 0.5956

15		0.315266	-441.668588	3.025223584	0.192428	120.75049	2.15577 1.09041 0.96914	X= 0.0522 Y= -1.2696 Z= -0.3874
16		0.295228	-441.668526	3.064129177	0.192426	120.74893	2.30374 1.05452 0.85865	X= 0.1389 Y= 0.1773 Z= 1.4978
17		0.125986	-441.667722	3.568646862	0.192538	120.81956	2.81595 0.90282 0.80228	X= -0.2307 Y= -1.4804 Z= -0.5694
18		0.121016	-441.667684	3.592492225	0.192667	120.90033	2.06943 1.16531 0.97326	X= -0.0783 Y= -0.4267 Z= 1.0498
19		0.10456	-441.667546	3.679088544	0.192963	121.08608	2.34636 1.07119 0.85721	X= 0.7955 Y= 5.0015 Z= 0.3346
20		0.069545	-441.667161	3.920679725	0.192619	120.87009	2.40951 1.03877 0.93494	X= -0.5103 Y= 0.3383 Z= 1.4094
21		0.06737	-441.667131	3.939505011	0.192642	120.88469	2.06351 1.18008 0.99177	X= 0.2451 Y= -0.1031 Z= -1.5767
22		0.054567	-441.666932	4.064379414	0.192971	121.09113	2.26378 1.07697 0.94105	X= -2.1888 Y= 4.3355 Z= 2.3058

23		0.031094	-441.666401	4.397586989	0.192565	120.83654	2.17556 1.07501 0.97363	X= -0.0046 Y= 0.9597 Z= 1.2679
24		0.009276	-441.665259	5.114202906	0.193228	121.25234	2.17673 1.17690 0.98240	X= -0.0319 Y= 5.0759 Z= -0.5516
25		0.003933	-441.664449	5.622485649	0.192801	120.98430	2.00462 1.27880 1.05870	X= 0.1237 Y= -0.9561 Z= 0.9415
26		0.002977	-441.664186	5.787520663	0.193391	121.35491	2.09459 1.25102 1.05711	X= -3.1887 Y= 4.2818 Z= 0.9250
27		0.000954	-441.663112	6.461465929	0.192765	120.96171	2.23528 1.16156 1.01494	X= 0.0471 Y= 0.3966 Z= -1.3004

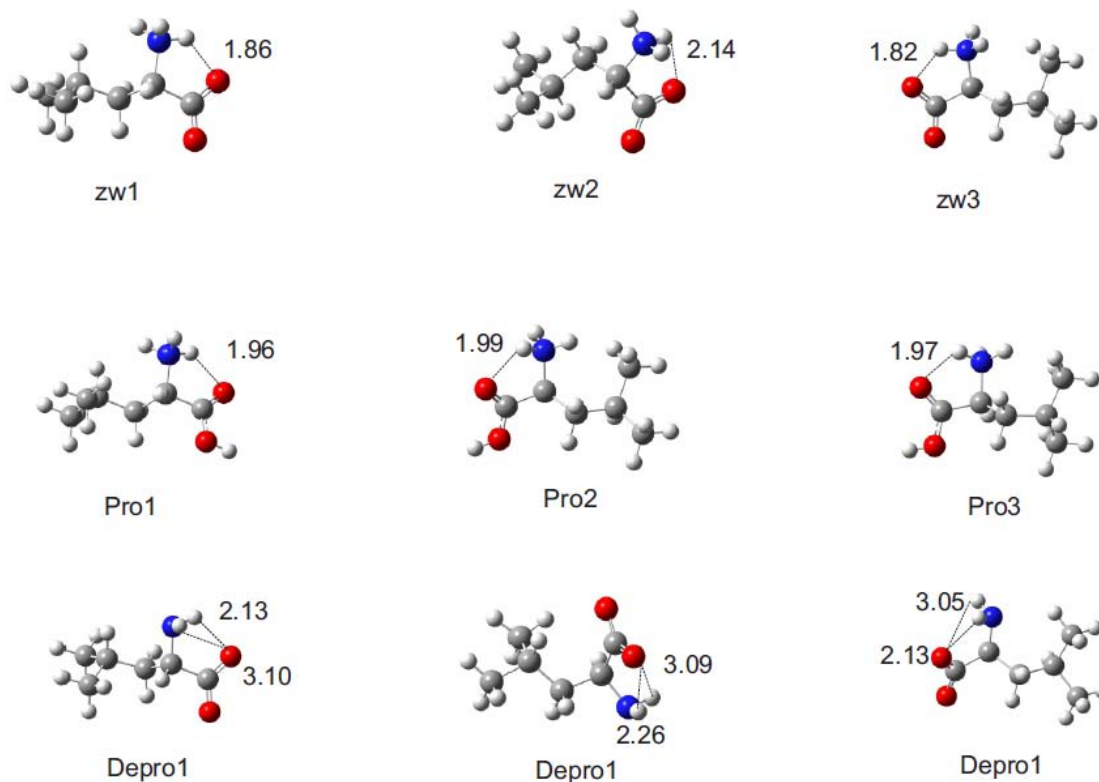


Figure 4.3 Optimized geometries of the three lowest energy conformers of the zwitterionic, deprotonated, and protonated monomeric leucine conformers at the B3LYP/6-311++G(d,p) level. The intermolecular hydrogen-bonding and secondary hydrogen-bonding interaction bond lengths are indicated.

4.4.2.2 Conformers of zwitterionic, deprotonated, and protonated leucine with water

Because most biologically important reactions involving amino acids happen in aqueous solution, it is essential to consider the effects of water on the conformational distribution of leucine. I have used the Polarized Continuum Model (PCM) for implicit solvation and also constructed the leucine-water complexes for explicit hydrogen bonding interaction between leucine and water. The preliminary results obtained are summarized below.

For the zwitterionic leucine monomer calculation, the geometries of the conformers obtained were re-optimized using a PCM of water at the B3LYP/6-311++G** level. Similarly, the geometry optimizations were also performed with PCM of water for the protonated and deprotonated leucine monomers. The relative total energies ΔE (kcal/mol) and the relative Gibbs free energies ΔG (kcal/mol) of the zwitterionic, deprotonated, and protonated leucine-water PCM calculation at the B3LYP/6-311++G(d,p) level of theory and their percentage Boltzmann distributions are summarized in Table 4.2. The Boltzmann population percentage was calculated using the follow formula:

$$P(i) = \frac{\exp\left[-\frac{\Delta G(i)}{RT}\right]}{\sum_i \exp\left[\frac{\Delta G(i)}{RT}\right]}$$

The corresponding values obtained for the conformers in the gas phase are also given in Table 4.2 in brackets for comparison. From the calculations, one can see that the dominant structure in the gas phase is still the most stable structure with PCM of water. The population percentage drops dramatically for the next and subsequent stable conformers. The simulated VA and VCD spectra of the three most stable conformers of leucine with PCM of water are

shown in Figure 4.4, 4.5, and 4.6 for the zwitterionic, protonated, and deprotonated leucine species, respectively.

Table 4.2 The relative total energies ΔE (kcal/mol) and the relative Gibbs free energies ΔG (kcal/mol) of the zwitterionic, deprotonated, and protonated leucine with PCM of water at the B3LYP/6-311++G(d,p) level of theory and their percentage Boltzmann distributions. The gas phase numbers are in brackets.

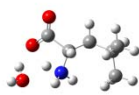
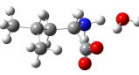
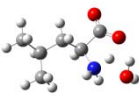
System	ΔE	$B_f(\Delta E)$	ΔG	$B_f(\Delta G)$
ZW1	1.49 (0)	6.96 (61.00)	0 (0)	93.89 (72.35)
ZW2	0 (0.55)	85.52 (24.17)	1.82 (0.86)	4.33 (17.02)
ZW3	1.44 (0.84)	7.52 (14.83)	2.35 (1.14)	1.78 (10.63)
DEP1	0 (0)	89.36 (53.19)	0 (0)	86.54 (65.42)
DEP2	1.66 (0.18)	5.46 (7.32)	1.12 (0.57)	13.08 (25.19)
DEP3	1.69 (1.18)	5.18 (7.32)	3.22 (1.15)	0.38 (9.39)

PRO1	0 (0)	98.03 (66.63)	0 (0)	98.87 (80.57)
PRO2	2.38 (0.64)	1.77 (22.81)	2.71 (1.02)	1.02 (14.40)
PRO3	3.69 (1.09)	0.19 (10.56)	4.00 (1.64)	0.11 (5.03)

To consider the explicit solvation with water, I also constructed leucine-water complexes. I use the most stable conformer as the starting point for all three leucine species. In Table 4.3, the possible conformers of the leucine-water complex are summarized. This is only the first step since leucine has several functional groups which are capable of hydrogen bonding to water molecules. Further theoretical modeling is needed to systematically account for such interactions properly.

Table 4.3 Summary of the possible zwitterionic leucine-water conformers

Name	Structures	Energy G (hartree)	ΔG (kcal/mol)	Population %	ΔZPE (hartree)	ΔZPE (kcal/mol)	Rotational Constants	Dipole Moments
5		-518.101930	2.066388978	2.045633	0.216435	135.8150314	2.03659 0.69907 0.61958	X= 0.9223 Y= -7.0139 Z= -0.3018

4		-518.102636	1.623367229	4.320987	0.216268	135.7102373	1.71860 0.70377 0.59188	X= 4.2105 Y= -5.9701 Z= 0.1036
8		-518.096971	5.178208881	0.010708	0.217790	136.6653069	2.09655 0.70331 0.63827	X= -0.5835 Y= -7.0270 Z= 0.0566
3		-518.103412	1.136419811	9.829642	0.216891	136.1011758	2.20046 0.62266 0.58506	X= 0.2670 Y= -6.7569 Z= 1.3251
7		-518.096998	2.066388978	0.011019	0.216148	135.6349362	1.26873 1.04841 0.84676	X= -3.4163 Y= 3.1784 Z= 5.1356
9		-518.096410	5.530241743	0.005911	0.218450	137.0794632	1.97831 0.69998 0.63329	X= -0.0479 Y= -7.3717 Z= -1.1655
6		-518.101347	2.432227051	1.103093	0.216952	136.13923	2.02075 0.70364 0.62458	X= -0.8475 Y= -6.0637 Z= -3.3075
2		-518.103857	0.857178058	15.74834	0.216155	135.63923	1.90465 0.65413 0.52877	X= -3.5886 Y= -6.3347 Z= -0.0417

1	 -518.105223	0	66.92457	0.216129	135.62309	1.91545 0.62125 0.55245	X= 3.4204 Y= -6.3933 Z= -1.1267
---	--	---	----------	----------	-----------	-------------------------------	---------------------------------------

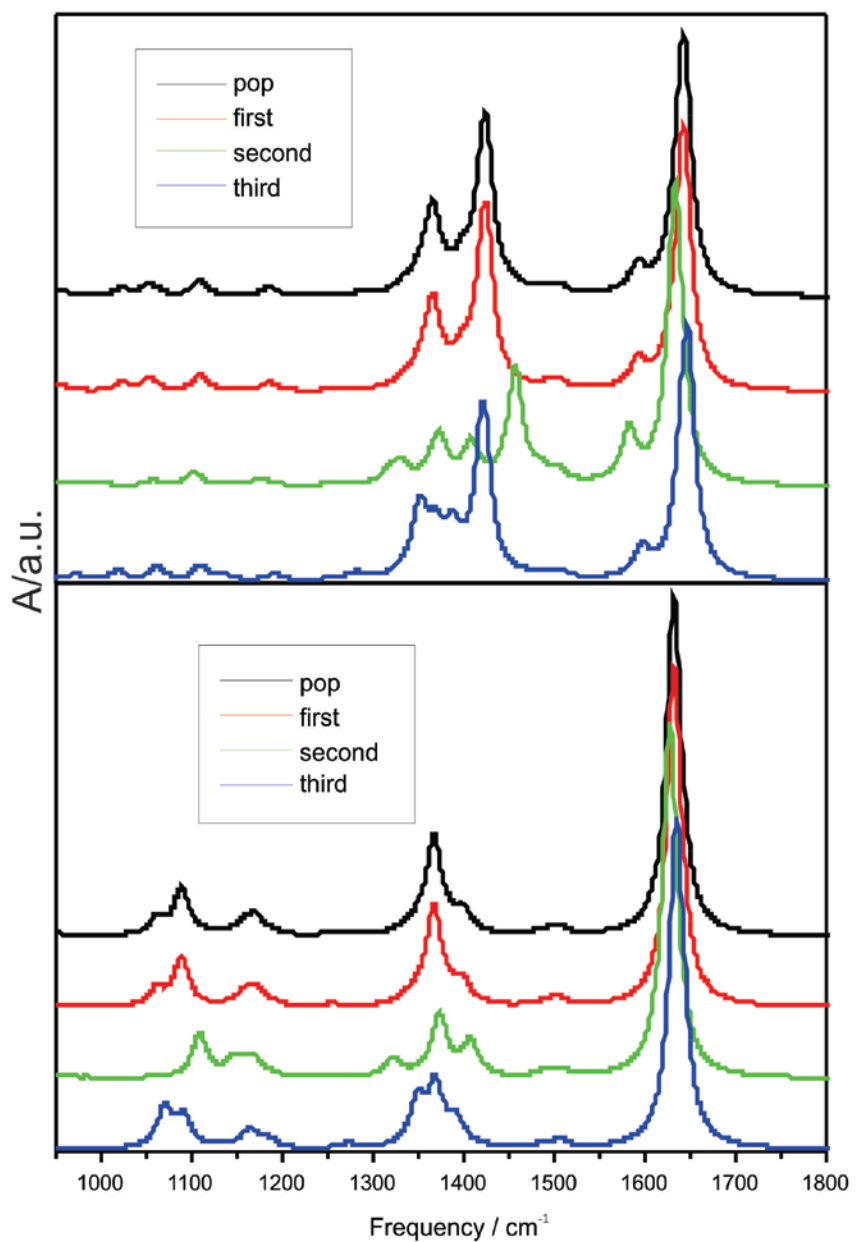


Figure 4.4 Simulated VA spectra of PCM of the three most stable zwitterionic leucine (top) and three most stable deuterated zwitterionic leucine (bottom) conformers at the B3LYP/6-311++G(d,p) level.

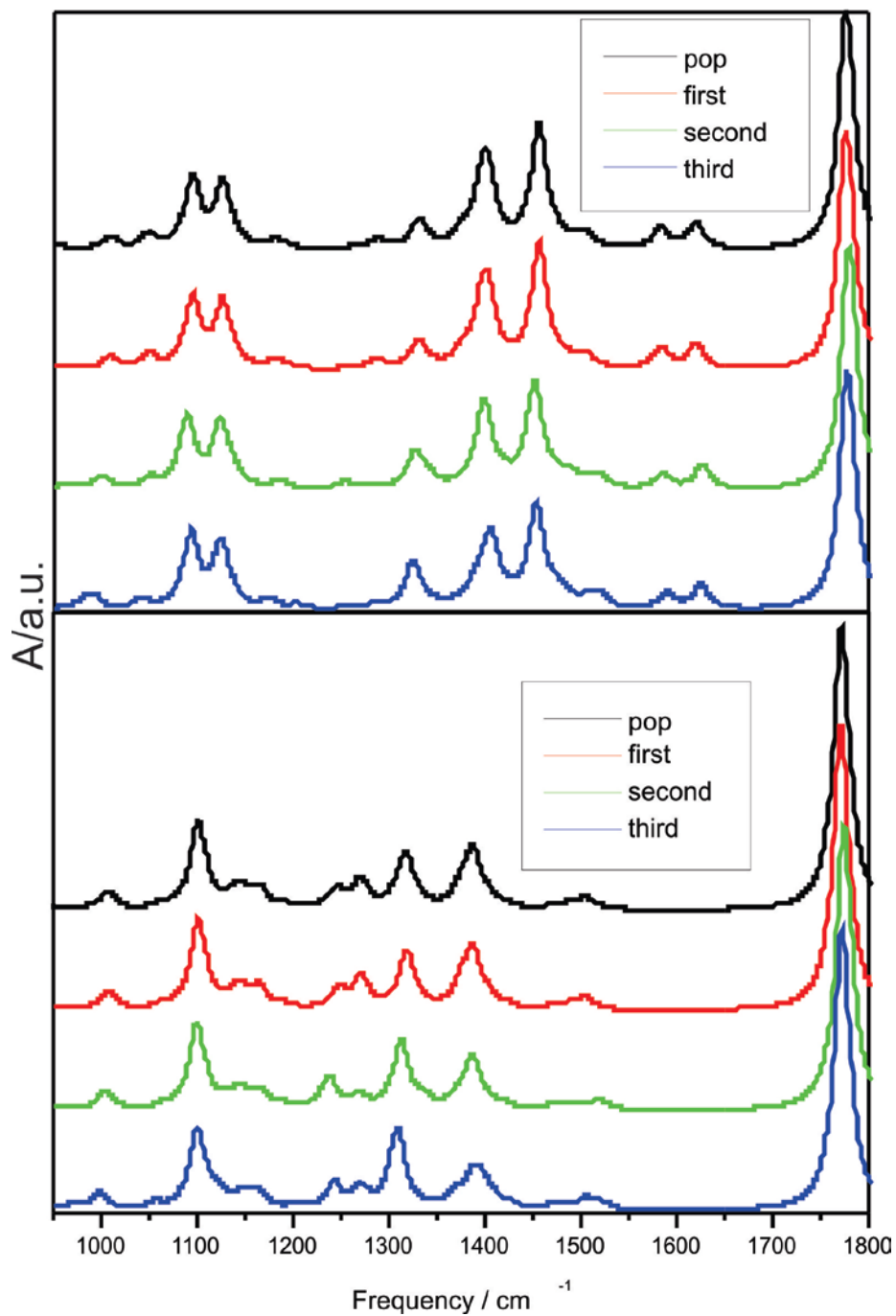


Figure 4.5 Simulated VA spectra of PCM of the three most stable protonated leucine (top) and three most stable deuterated protonated leucine (bottom) conformers at the B3LYP/6-311++G(d,p) level.

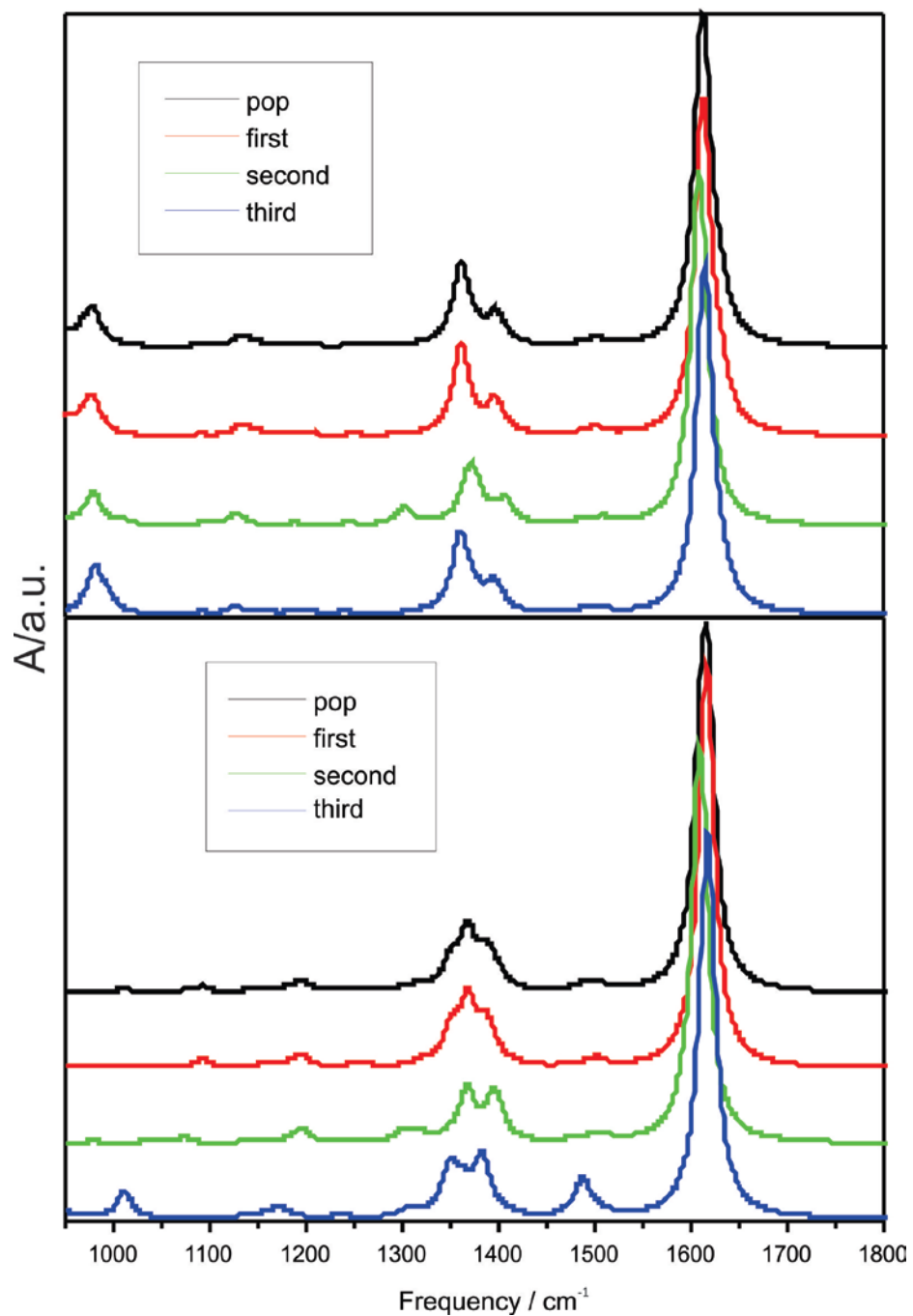


Figure 4.6 Simulated VA spectra of PCM of the three most stable deprotonated leucine (top) and three most stable deuterated deprotonated leucine (bottom) conformers at the B3LYP/6-311++G(d,p) level.

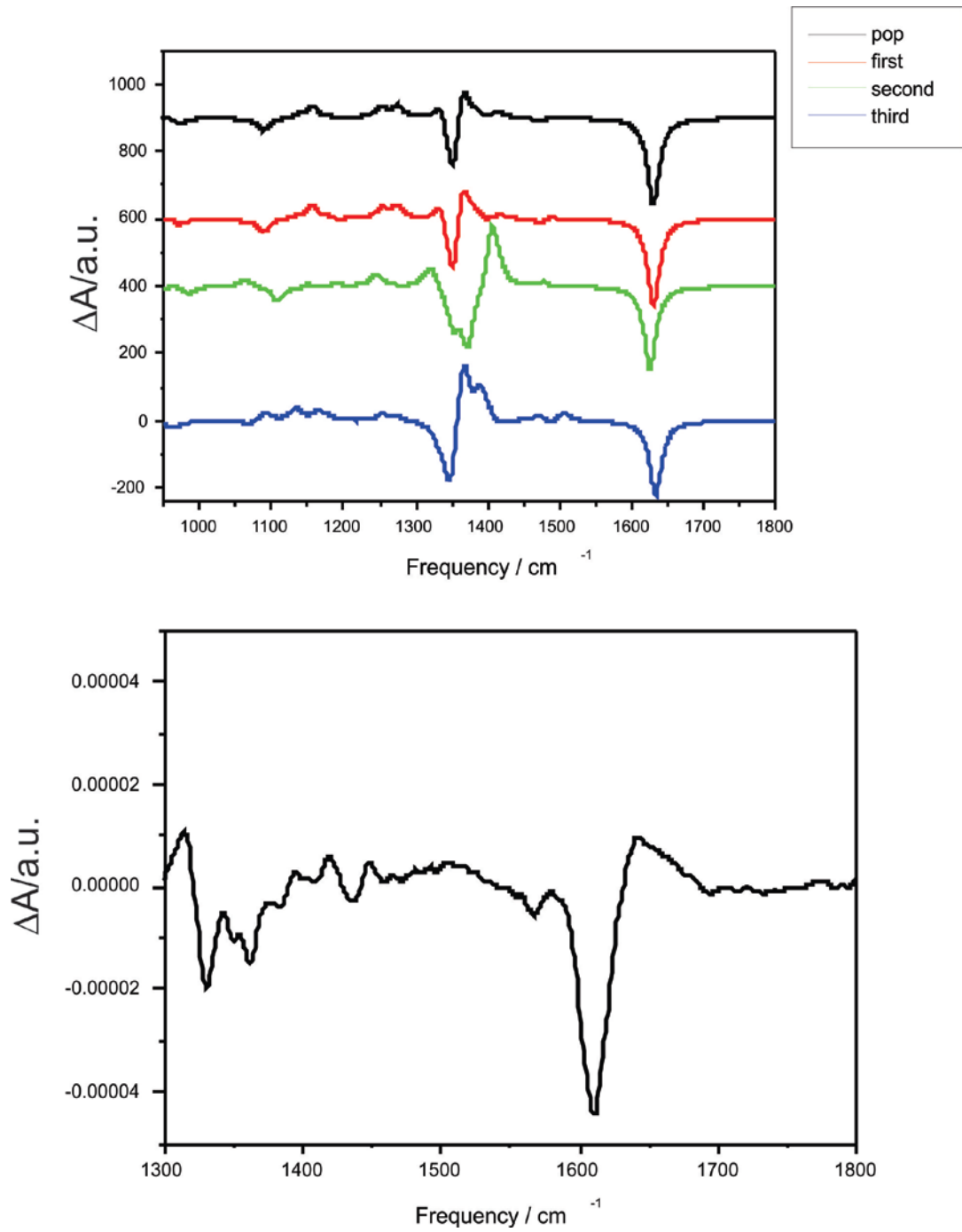


Figure 4.7 Comparison of VCD spectra of leucine in D₂O using PCM of leucine with water.

4.5 Conclusion

In this project, the dominant species and the conformational distributions of leucine under three representative pHs, i.e., strongly acidic, near neutral, and strongly basic conditions, have been investigated using VA and VCD spectroscopy, complemented with *ab initio* calculations. It has been found that the dominant species are the deprotonated, zwitterionic, and a mixture of the protonated and zwitterionic forms of leucine under strongly basic, near neutral, and strongly acidic conditions, respectively. Based on the gas phase simulations of one of the most stable conformers of zwitterionic, protonated, and deprotonated species, the experimental VA and VCD spectra could be interpreted, although there are notable discrepancies (see Fig 4.7). Inclusions of the water solvent by PCM and by the explicit leucine-water hydrogen-bonding interactions have been performed as the first steps to properly account for the effects of water solvent. Further systematic theoretical study is needed for this project. In particular, it was recently reported by our group¹² that a combined explicit and implicit solvation model when both the hydrogen bonding of leucine with water molecules and the effects of bulk water were taken into account simultaneously provides excellent agreement with the experimental data.

References:

1. (a) G. Albrecht, R.B. Corey, *J. Am. Chem. Soc.* 61 (1939) 1087. (b) P.G. Jonsson, A. Kvick, *Acta Cryst. B* 28 (1972) 1827. (c) Y. Ding, K. Krogh-Jespersen, *Chem. Phys. Lett.* 199 (1992) 261. (d) F.R. Tortonda, J.L. Pascual-Ahuir, E. Silla, I. Tunonon, F.J. Ramirez, *J. Chem. Phys.* 109 (1998) 592.
2. J. Rosenthal, A. Angel, J. Farkas, Department of Medicine, University of Toronto, Toronto, Canada. "Metabolic fate of leucine: A significant sterol precursor in adipose tissue and muscle". *American Journal of Physiology Vol. 226, No. 2, p. 411-418.*
<http://ajplegacy.physiology.org/cgi/reprint/226/2/411>. Retrieved 2008-03-25.
3. (a) Timothy A. Keiderling *CURRENT OPINION IN CHEMICAL BIOLOGY* 6 , 682-688, 2002 (b) Pizzanelli, Silvia; Forte, Claudia; Monti, Susanna; Zandomeneghi, Giorgia; Hagarman, Andrew; Measey, Thomas J; Schweitzer-Stenner, Reinhard *J Phys Chem B*, 114, 3965-3978, 2010 (c) Seongeun Yang; Minhaeng Cho, *Journal of Chemical Physics*, 131, 135102, 2009. (d) Schweitzer-Stenner *R JOURNAL OF PHYSICAL CHEMISTRY B* 113, 2922-2932, 2009.
4. (a) P. J. Stephens, F. J. Devlin, C. F. Chabalowski, M. J. Frisch, *J. Phys. Chem.* 98, 11623 (1994). (b) T. Kuppens, W. Langenaeker, J. P. Tollenaere, P. Bultinck, *J. Phys. Chem. A* 107, 542 (2003). (c) T. Kuppens, K. van der Vandyck, J. Eycken, W. Herrebout, B. J. van der Veken, P. Bultinck, *J. Org. Chem.* 70, 9103 (2005). (d) T. Kuppens, W. Herrebout, B. van der Veken, P. Bultinck, *J. Phys. Chem. A* 110, 10191 (2006). (e) Ducasse, F. Castet, A. Fritsch, I. Huc, T. Buffeteau, *J. Phys. Chem. A* 111, 5092 (2007). T. Brotin, D. Cavagnat, J.-P. Dutasta, T. Buffeteau, *J. Am. Chem. Soc.* 128, 5533 (2006)..
5. (a) W. Sander, M. Gantenberg, *Spectrochim. Acta A* 62, 902 (2005). (b) A. K. Chandra, S. Parveen. T. Zeegers-Huyskens, *J. Phys. Chem. A* 111, 8884 (2007). (c) J. N. Woodford, *J. Phys. Chem. A* 111, 8519 (2007). (d) P. I. Dem'yanov, R. M. Gschwind, *ORGANOMETALLICS*, 25, 5709 (2006).
6. Frisch, M. J.; Trucks, G. W.; Schlegel, H. B.; Scuseria, G. E.; Robb, M. A.; Cheeseman, J. R.; Montgomery, J. A., Jr.; Vreven, T.; Kudin, K. N.; Burant, J. C.; Millam, J. M.; Iyengar, S. S.; Tomasi, J.; Barone, V.; Mennucci, B.; Cossi, M.; Scalmani, G.; Rega, N.; Petersson, G. A.; Nakatsuji, H.; Hada, M.; Ehara, M.; Toyota, K.; Fukuda, R.; Hasegawa, J.; Ishida, M.; Nakajima, T.; Honda, Y.; Kitao, O.; Nakai, H.; Klene, M.; Li, X.; Knox, J. E.; Hratchian, H. P.; Cross, J. B.; Bakken, V.; Adamo, C.; Jaramillo, J.; Gomperts, R.; Stratmann, R. E.; Yazyev, O.; Austin, A. J.; Cammi, R.; Pomelli, C.; Ochterski, J. W.; Ayala, P. Y.; Morokuma, K.; Voth, G. A.; Salvador, P.; Dannenberg, J. J.; Zakrzewski, V. G.; Dapprich, S.; Daniels, A. D.; Strain, M. C.; Farkas, O.; Malick, D. K.; Rabuck, A. D.; Raghavachari, K.; Foresman, J. B.; Ortiz, J. V.; Cui, Q.; Baboul, A. G.; Clifford, S.; Cioslowski, J.; Stefanov, B. B.; Liu, G.; Liashenko, A.; Piskorz, P.; Komaromi, I.; Martin, R. L.; Fox, D. J.; Keith, T.; Al-Laham, M. A.; Peng, C. Y.;

Nanayakkara, A.; Challacombe, M.; Gill, P. M. W.; Johnson, B.; Chen, W.; Wong, M. W.; Gonzalez, C.; Pople, J. A. Gaussian03, revision C.02; Gaussian, Inc.: Wallingford, CT, 2004.

7. R. M. C. Dawson, D. C. Elliott, W. H. Elliott, K. M. Elliott, K. M. Jones, *Data for biochemical research*. Oxford Science. New York. 1986
8. E. J. Cocinero, A. Lesarri, J. Grabow, J. C. López, and J. L. Alonso, *J. Phys. Chem.* 2007, **8**, 599-604.
9. A. D. Becke, *J. Chem. Phys.*, 1993, **98**, 5648-5652.
10. C. T. Lee, W. T. Yang, R. G. Parr, *Phys. Rev. B*, 1988, **37**, 785-789.
11. M. Noguera, L. Rodríguez-Santiago, M. Sodupe, and J. Bertran, *J. Mol. Struct. (Theo.)*, 2001, **537**, 307-318.
12. M. R. Poopari, Z. Dezhahang, G. Yang, and Y. Xu, *Chem. Phys. Chem*, 2012 (accepted).

Chapter 5

General Conclusions and future work

In this thesis, I summarize the research I have been involved in during my tenure as a physical chemistry student. My master research focuses on the conformational distributions of amino acids in aqueous solution. The study of serine is described in chapter 3 and while that of leucine in chapter 4.

The detailed conformational distributions of the dominant serine species under three representative pHs, i.e., strongly acidic, near neutral, and strongly basic conditions, have been investigated using VA and VCD spectroscopy, together with ab initio calculations and MD simulations. Although the observed VA and VCD spectra can be interpreted roughly based on the gas phase simulations of the most stable conformers of the protonated, deprotonated and zwitterionic serine species, it was difficult to draw concrete conclusion without taking water solvent into account. To improve the agreement between experiment and theory, both PCM implicit and explicit hydrogen-bonding interaction models have been considered. The inclusion of the explicit serine-water hydrogen-bonding interactions was found to improve the agreements between the experimental and simulated VA and VCD spectra noticeably in all the cases examined here. This, together with the availability of the experimental VA and VCD spectra in both H₂O and D₂O, allowed us to identify the dominant conformers confidently.

In the leucine project, similar experimental and theoretical approaches have been used as in the serine project. Because of time constraint, only preliminary theoretical modelling has been completed. Further calculations are still needed to have a better understanding of the experimental spectra since the agreement between the current simulated VA and VCD spectra and the experimental data is still not satisfactory. To further improve the agreement between experiment and theory, it may be necessary to consider both explicit and implicit solvation models simultaneously. Especially for the leucine project, some new simulations including both explicit and implicit solvation models simultaneously are currently being performed by another student in our group. The preliminary results from these further efforts show noticeably improvements over what we had achieved so far with the explicit model. Nevertheless, based on the current calculations, we understand that accurate description of the intramolecular interaction in leucine and intermolecular interaction between leucine and water is very important for a detailed understand of conformational distributions of serine or leucine in water.

The present report demonstrates that VCD spectroscopy in combination with quantum chemistry and molecular dynamics calculations is an attractive new tool to analyze the conformational distribution of amino acids in aqueous solution under different pH conditions. Such tool also allows us to explore the mechanism of solvation of highly flexible chiral molecules and helps us to quantify the hydrogen bonding interactions in these systems.